A Two-Dimensional Variational Analysis Method for NSCAT Ambiguity Removal: Methodology, Sensitivity, and Tuning

R. N. HOFFMAN, S. M. LEIDNER, AND J. M. HENDERSON

Atmospheric and Environmental Research, Inc., Lexington, Massachusetts

R. ATLAS

Data Assimilation Office, NASA Goddard Space Flight Center, Greenbelt, Maryland

J. V. ARDIZZONE AND S. C. BLOOM

Science Applications International Corporation, Beltsville, Maryland

(Manuscript received 8 October 2001, in final form 12 September 2002)

ABSTRACT

In this study, a two-dimensional variational analysis method (2DVAR) is applied to select a wind solution from NASA Scatterometer (NSCAT) ambiguous winds. A 2DVAR method determines a ''best'' gridded surface wind analysis by minimizing a cost function. The cost function measures the misfit to the observations, the background, and the filtering and dynamical constraints. The ambiguity closest in direction to the minimizing analysis is selected. The 2DVAR method, sensitivity, and numerical behavior are described. 2DVAR is used with both NSCAT ambiguities and NSCAT backscatter values. Results are roughly comparable. When the background field is poor, 2DVAR ambiguity removal often selects low probability ambiguities. To avoid this behavior, an initial 2DVAR analysis, using only the two most likely ambiguities, provides the first guess for an analysis using all the ambiguities or the backscatter data. 2DVAR and median filter-selected ambiguities usually agree. Both methods require horizontal consistency, so disagreements occur in clumps, or as linear features. In these cases, 2DVAR ambiguities are often more meteorologically reasonable and more consistent with satellite imagery.

1. Introduction

Scatterometers are active radars designed to measure the backscatter or normalized radar cross section (NRCS) from the earth's surface at moderate incidence angles. The advantage of using moderate incidence angles (20°–70°) is that the major mechanism for scattering is then Bragg scattering from centimeter-scale waves, which are, in most conditions, in equilibrium with the local wind. Although the scatterometer winds are usually provided as neutral winds at some reference height, the measurement is physically most closely connected with surface stress (Brown 1986).

Scatterometers measure wind speed very accurately; Freilich and Dunbar (1999) report that National Aeronautics and Space Administration (NASA) Scatterometer (NSCAT) measured wind speed to within 1.3 m s^{-1} in an rms sense, while Stoffelen and Anderson (1997b) suggest that the *ERS-1* measurement error standard deviation is actually only 0.5 m s^{-1}. However, the wind direction from scatterometers is not uniquely determined. Wind speed and direction are inferred from a number of closely collocated (both temporally and spatially) radar measurements from a number of different azimuth angles. The measured NRCS, denoted σ^0, varies with the relative azimuth angle between the antenna and wind direction. An ''upwind-crosswind'' variation exists because small, wind-generated gravity waves on the ocean surface reflect more of the radar signal when wave crests are perpendicular (i.e., ''upwind'') to the radar antenna than when wave crests are parallel (i.e., ''crosswind''). The ''upwind–downwind'' signal is very small, because when fetch is not limited, the orientation and amplitude of these waves is nearly the same if the wind direction is shifted by 180°.

This paper reports on the use of a two-dimensional variational analysis method (2DVAR) for removing the directional ambiguity of NSCAT winds. 2DVAR generates a gridded surface wind analysis by minimizing an objective function, which is a weighted sum of several constraints on the difference between the analysis

Corresponding author address: Dr. Ross N. Hoffman, Atmospheric and Environmental Research, Inc., 131 Hartwell Ave., Lexington, MA 02421-3126.
E-mail: rhoffman@aer.com

and the background, and between the analysis and the data. While the ''nudged'' median filter uses a priori information for initialization, 2DVAR uses such information both for initialization and as part of the background constraints. 2DVAR was originally described by Hoffman (1982) to analyze *Seasat* scatterometer (SASS) data. In this first formulation, only observations from conventional platforms (ships, buoys, radiosondes) and from SASS were combined with an a priori or background wind field. 2DVAR was extended to include smoothness (i.e., filtering) constraints and a dynamical constraint by Hoffman (1984, hereafter H84). This study extends the ambiguity method of H84 to use NSCAT data, to use σ^0 as an alternative to ambiguities, and to use dual ambiguity processing as an initial step. Dual ambiguity processing makes use of the relative likelihoods of the ambiguities to avoid problems due to gross directional errors in the background wind field.

Our approach to data analysis in 2DVAR is heuristic, starting with the simple premise that the desired analysis closely fits the available data and simultaneously closely satisfies certain constraints that have a clear physical interpretation. The 2DVAR constraints state that the analysis should be close to the background, that the analysis increments should be smooth, and that the analyzed dynamical balance be close to that of the background. The first two are generic constraints that could be applied to any problem, while the third is specifically applicable to a surface wind field. 2DVAR is thus an extension of the thin plate spline approach described by Wahba and Wendelberger (1980). In such approaches one must specify relative weights for the individual constraints. In the simplest case there is only one relative weight that controls the trade-off between fidelity to data and smoothness. This parameter (or a small set of such parameters) may be chosen on a case-by-case or ensemble basis using the method of generalized cross validation (Gu and Wahba 1991; Wahba et al. 1995) and approximations thereof (Desroziers and Ivanov 2001). As a result, 2DVAR is an ideal candidate for online estimation of parameters as Dee and da Silva (1998) and Dee et al. (1999) have proposed. This feature of 2DVAR has been exploited by Pegion et al. (2000) to objectively tune these parameters. In the work described here, these parameters are chosen subjectively based on experimentation.

The outline of the rest of this paper is as follows. First we define the NSCAT data and the usual processing of the NSCAT data (section 2). We then describe the 2DVAR methodology for conventional data and for NSCAT data, and discuss the numerical behavior and the sensitivity of 2DVAR (section 3). We have improved the quality of our ambiguity removal by using a first stage in which only ''dual ambiguities'' are processed. This method and our other quality control procedures are presented in section 4. Experiments using ambiguities and σ^0 values are compared. With proper tuning the results are similar (section 5). Examples of our dual-ambiguity quality control (dual QC) method in 2DVAR are shown in section 6. Then section 7 is a conclusion. In a companion article (Henderson et al. 2003) the dual-QC 2DVAR is applied to the entire NSCAT mission and 2DVAR ambiguity removal is compared to results from the ''nudged'' median filter.

2. NSCAT data

Scatterometers have been mounted on stationary platforms, aircraft, and satellites. Since 1991, satellite-borne scatterometers have provided a wealth of wind data over the World Ocean. Previous satellite scatterometers include *Seasat-A* Satellite Scatterometer in 1979; the active microwave instruments on the first and second European Remote Sensing satellites (*ERS-1* and *ERS-2*), during 1991–2000; and the NASA Scatterometer (NSCAT) on the first Advanced Earth Observing Satellite (*ADEOS-1*) during 1996–97. Since 1999, SeaWinds on QuikSCAT has been operational.

The focus of this study is winds retrieved from NSCAT. NSCAT was launched aboard the *ADEOS-1* spacecraft on 16 August 1996 from Tanegashima Space Center in Japan. Unfortunately, after only 9 months of operation, the *ADEOS-1* solar power array failed. *ADEOS-1* had a nearly polar sun-synchronous orbit at a height of ~800 km, with a period of ~100 min.

NSCAT made observations covering two 600 km swaths, one on either side of the spacecraft, separated by a gap of ~330 km corresponding to low incidence angles. On each side of the spacecraft, NSCAT operated three 3-m-long, sticklike antennas at 13.995 GHz. The foreward and aft antennas were vertically polarized, while the mid antenna was both vertically and horizontally polarized. Thus NSCAT made observations in sequence from eight beams, that is, from eight combinations of antennas and polarizations. While the foreward and aft antennas are separated by 90° as in the *ERS-1* design, the angles between the mid antenna and the others are 20° and 70°, whereas in the *ERS-1* design these angles are 45°. The NSCAT antenna subsystems, resolution, registration of observations, measurement sequencing, hardware, and ground system are described by Naderi et al. (1991).

Key components of the ground system are modeling the backscatter measurements, wind retrieval, and ambiguity removal. Geophysical model functions are empirical relationships used to relate the backscatter to the geophysical parameters, and are usually derived from collocated observations (Jones et al. 1977). In current model functions, the backscatter depends nonlinearly on wind speed and direction. Models developed from aircraft flights have been used as baseline model functions for satellite instruments. However, substantial postlaunch modifications and refinements were needed for SASS (Boggs 1981) and for *ERS-1* (Offiler 1994; Stoffelen and Anderson 1997b). The prelaunch NSCAT model function, denoted NSCAT-0 or SASS2, was de-

veloped by Wentz et al. (1984) from the *Seasat* dataset by matching the statistics of the observed σ^0 and those simulated assuming that the ocean surface winds follow a one parameter Weibull distribution (Conradsen et al. 1984). The fitting procedure used six parameters at each polarization and incidence angle. The first postlaunch NSCAT model function, denoted NSCAT-1, was developed using a combination of Special Sensor Microwave Imager (SSM/I), National Centers for Environmental Prediction (NCEP), and European Centre for Medium-Range Weather Forecasts (ECMWF) winds collocated with NSCAT σ^0 observations. A further refinement, denoted NSCAT-2, has been developed by Wentz and Smith (1999), based on collocations with SSM/I and ECMWF winds.

In the ground processing, the individual backscatter observations associated with the different beams are organized by a grid oriented along the satellite track. Usually there are 4 or 16 backscatter observations in a 25- or 50-km wind vector cell (WVC). The WVC coordinates along, and perpendicular to, the satellite track are called row and cell, respectively. Each cell is associated with a nearly constant incidence angle for each antenna, with the values being equal for the fore and aft antennas. Modeled σ^0 values are computed from a geophysical model function that requires spacecraft position and orientation (known) and wind speed and direction (unknowns) as inputs. Within each WVC containing a sufficient number of quality controlled backscatter observations, the normalized squared differences between measured and modeled σ^0 values are summed as part of the objective function of a maximum likelihood estimator (MLE). Then, wind speed and direction are varied to maximize the likelihood. However, over the range of possible wind speeds and directions (i.e., 0–50 m s^{-1} and 0°–360°), the MLE produces from two to six local maxima, and it is not possible to determine the wind uniquely from the MLE alone. Examples of the likelihood function are described in section 3a. The wind vectors corresponding to the likelihood maxima are called ''ambiguities.'' The ambiguities are ordered by likelihood. The first ambiguity is the ambiguity with the highest likelihood; it is most consistent with the backscatter data. The second ambiguity is usually of nearly equal speed and consistency, but of nearly opposite direction.

For operational numerical weather prediction (NWP), and for other purposes, it is necessary to choose one ambiguity at each location in a meteorologically consistent manner. Once we have chosen a single ambiguity, we call the result a ''unique'' wind. Since the wind retrieval is performed for each WVC individually and since there is little to distinguish the first two ambiguities, a wind field of first ambiguities will generally be very irregular with many wind reversals. Spatial filtering can be used to produce a horizontally consistent wind field and resolve the directional ambiguity. A variety of approaches have been used. These include the work of H84, Schroeder et al. (1985), Schultz (1990), Shaffer et al. (1991), Wentz (1991), Badran et al. (1991), Offiler (1992), Thépaut et al. (1993a), Long (1993), Stoffelen and Anderson (1997a), Jones et al. (1999), Figa and Stoffelen (2000), and de Vries and Stoffelen (2000).

Simulation studies for NSCAT established that a median filter operating autonomously, that is, with no a priori information, would provide excellent ambiguity selection (Schultz 1990; Shaffer et al. 1991). The median filter must be initialized or seeded with some initial choice of ambiguities. In autonomous mode the seed is the first ambiguity. In practice this choice did not perform as well as expected. Better performance was obtained by initializing the scatterometer wind field with the ambiguity closest to the operational gridded surface wind field analysis from NCEP. This product is referred to as the nudged wind product since an outside source is used to initialize (or ''nudge'') the median filter. No further reference to the background is made. At the end of the process the chosen winds are consistent with backscatter observations in the WVC and horizontally consistent with neighboring WVCs, but are not necessarily close to the background. The median filter method has been quite successful (Gonzales and Long 1999). Differences between autonomous and nudged results show that the median filter has multiple solutions. Thus spatial filtering does not resolve all ambiguity in the sense that multiple horizontally consistent wind fields are plausible. Further, the median filter occasionally selects physically unrealistic winds. Patches of unrealistic winds in the scatterometer data might have a disastrous impact on the quality of analyses and NWP forecasts. Careful quality control (QC) is required, of course, but is problematic if the model winds were used in the ambiguity removal.

It should be noted that there are several NSCAT data products available. These differ in resolution (25 or 50 km); geophysical model function (NSCAT-0, NSCAT-1, or NSCAT-2), and ambiguity selection procedure (autonomous or nudged median filter). All Jet Propulsion Laboratory (JPL) NSCAT datasets use the median filter described by Shaffer et al. (1991). The 25-km resolution datasets based on the NSCAT-2 model function and the nudged median filter are the most current. Some of the preliminary results presented here, however, use other versions of the NSCAT data.

3. 2DVAR method

2DVAR finds the minimum of an objective function, denoted *J*. The objective function depends on the surface wind field. Given any wind field the objective function measures the difference between the given field and the observations, and between the given field and the a priori or background wind field. The minimizer of the objective function is therefore the wind field, which

optimally fits the observed and a priori data. We write the 2DVAR objective function as

$$J = J_b + J_o. \quad (1)$$

Here J is the total cost function, J_b is the background cost function, and J_o is the observation cost function. As in any analysis method, specification of the error characteristics of the data and the background are vitally important. Our implementation of 2DVAR employs a heuristic model of forecast error statistics. In this study,

$$J_b = \lambda_{\mathrm{VWM}} J_{\mathrm{VWM}} + \lambda_{\mathrm{LAP}} J_{\mathrm{LAP}} + \lambda_{\mathrm{DIV}} J_{\mathrm{DIV}} + \lambda_{\mathrm{VOR}} J_{\mathrm{VOR}} + \lambda_{\mathrm{DYN}} J_{\mathrm{DYN}}, \quad \text{and} \quad (2)$$

$$J_o = \lambda_{\mathrm{CONV}} J_{\mathrm{CONV}} + \lambda_{\mathrm{AMB}} J_{\mathrm{AMB}} + \lambda_{\mathrm{SPD}} J_{\mathrm{SPD}} + \lambda_{\mathrm{NRCS}} J_{\mathrm{NRCS}}. \quad (3)$$

Each constraint function, J_m, is a scalar that measures the difference between the analysis and background using the mth constraint. The constraints include filtering and dynamical consistency. The lambda weights, denoted λ_m, control the amount of influence each constraint has on the final analysis. It should be noted that these are weak constraints and therefore the λ_m are not Lagrangian multipliers. The constraint function subscripts are mnemonics: J_{VWM} is the background constraint on the vector wind magnitude, J_{LAP} on the Laplacian of the wind components, J_{DIV} on the divergence, and J_{VOR} on the vorticity; J_{DYN} is the dynamic constraint on the vorticity tendency; and J_{CONV} is the observation function for the conventional data, J_{AMB} for the ambiguous winds, J_{SPD} for the scatterometer wind speed, and J_{NRCS} for the backscatter.

Details of the calculation of J_o and J_b and the behavior of 2DVAR are given in the following sections and in the appendices. The combination of the J_m constraints in (2) mimicks the usual J_b term in 3D-VAR or 4D-VAR (e.g., Thépaut et al. 1993b). Therefore, 2DVAR as described here may be considered to be a specialization of 3D-VAR to ocean surface wind. The approach we have taken in developing the 2DVAR may seem very different than the usual approach in data analysis. There are in fact a number of parallels to the usual approach. However, in formal approaches, the underlying assumptions and tuning may not be as apparent as in our exposition of 2DVAR. The validity of the assumptions and the appropriateness of the tuning are critical to the success of the methods. In a formal approach, one begins by seeking the maximum likelihood estimate as calculated by Bayes' theorem. For a linear problem, if the various errors have a zero mean Gaussian distribution, then the MLE is the best unbiased linear estimator in the strict statistical sense. However, these assumptions are usually not realized. The next difficulty is in estimating the various statistical quantities that define the MLE. Simplifying assumptions must be made. Although the statistics no doubt depend on synoptic situation, season, latitude, time of day, topography, etc., data samples are rarely of sufficient size and quality for anything more than a cursory stratification. It is not unusual to make one's best attempt at specifying the statistics, and then to introduce a scaling, or then to tune certain parameters in the models of the statistics in order to get subjectively agreeable results.

As mentioned in section 1, the λ_m values are chosen subjectively in this study, but techniques to tune them objectively have been developed. Values of the λ_m that were used for various experiments are reported below. After subjective tuning, the 2DVAR heuristic model of forecast error statistics produces results similar to conventional error models, but has the potential advantage of being specified by a small number of parameters. In principle, these parameters might vary with geographic location, with synoptic situation and might even be tuned online, using current or recent data. We choose these parameters subjectively based on experimentation. However, some of our results address how to tune these parameters to get similar results when changing the analysis resolution, data density, or data representation (see section 5).

Since H84 2DVAR has undergone several developments. These include the optional use of 12-point bicubic interpolation to the observation locations (section 3a), the use of σ^0 values (section 3a), and the reformulation of the constraint terms (section 3b). 2DVAR may combine both wind retrieval and ambiguity removal by analyzing the σ^0 data directly. For both *ERS-1,-2* and NSCAT, in addition to the possibility of analyzing σ^0 data, the ambiguities may be treated in the same manner as SASS data were treated by H84, or unique winds may be treated as buoy observations. 2DVAR has been used to produce several long running datasets for oceanographic research. First, 2DVAR was adapted for use with time-binned wind observations by Florida State University researchers including Legler et al. (1989), Meyers et al. (1994), Jones et al. (1995), and Pegion et al. (2000). Later, 2DVAR was extended to SSM/I wind magnitude data by Atlas et al. (1991, 1996).

The order of the steps taken in 2DVAR is flexible and the subject of ongoing tuning. The usual and minimal preparation for the minimization is to define the geometry of the analysis grid, and on this grid the background wind field, and the initial estimate for the analysis; to read the observation datasets, making necessary conversions and performing gross QC; and to quality control the observation based on simulated values from the background. These preparations may be modified in several ways. The initial estimate is usually equal to the background, but may be an arbitrary wind field. For example, after a preliminary analysis, the analysis and background can be interpolated to a finer grid. Also, after a preliminary analysis, all data may be subjected to a second QC, accepting some data that were initially rejected but are corroborated by nearby data. In these cases the minimization restarts, using the preliminary

analysis as the initial estimate. The dual-QC approach of section 4c is a similar modification.

In order to minimize the objective function J we must be able to calculate it for any physically reasonable value of the control variable vector $\mathbf{X}$, which here represents the surface wind field. We must specify the mapping $\mathcal{M}$,

$$\mathbf{V}_a = \mathcal{M}(\mathbf{X}), \tag{4}$$

from the control vector $\mathbf{X}$ to a complete gridded wind field $\mathbf{V}_a$. In the current formulation $\mathbf{X}$ contains those values of the gridded wind components (u, v) that are independent and free to vary. Not all points in the gridded wind fields are allowed to vary. Such fixed points at or near the boundaries are part of $\mathbf{V}_a$ but are not part of $\mathbf{X}$. Note that $\mathbf{V}_a$ is the 10-m neutral stability wind field and that all observed winds should be translated into a 10-m neutral stability wind. If only the height of the observation is known, then the neutral logarithmic wind profile may be used to adjust the wind observation to 10 m.

Efficient minimization also requires the calculation of the gradient of J, that is, $\partial J/\partial \mathbf{X}$. This is accomplished by the adjoint of the routines that calculate J (Hoffman et al. 1992). The minimization procedure we use is a version of the limited-memory quasi-Newton algorithm (Liu and Nocedal 1989), which was described and evaluated by Navon and Legler (1987). The algorithm iterates until the size of $\partial J/\partial \mathbf{X}$ is small—smaller than ϵ times the size of $\mathbf{X}$—or until a maximum number of function evaluations have been used, whichever occurs first.

We have been unsuccessful at preconditioning the minimization. Usually several hundred iterations are required to satisfy our very strict convergence criterion. In a typical experiment the rms difference in the u or v wind components between the solution after 250 and after 225 function calls is $\sim$0.02 m s^{-1}, with maximum differences of $\sim$0.5 m s$^{-1.}$ Our experiments use relatively small samples and computer timings are sufficiently fast. The reason for the slow convergence is due to the step-by-step expansion of the region of influence of the data (section 3c). A regridding process speeds convergence (appendix B2). An operational implementation might use less strict convergence criteria, and regrid or possibly remap the control vector $\mathbf{X}$ into spectral space to increase efficiency. With a spectral representation, the mapping from $\mathbf{X}$ to $\mathbf{V}_a$ would be more complicated, but some of the J_b terms would be easier to calculate, and the minimization might converge more quickly.

a. Observation functions

In general, the total observation function J_o is the weighted sum of individual observation operators for each data class. The data classes are defined for convenience. For example, we might divide ships into special research ships and all others, and buoys into Tropical Atmosphere–Ocean buoys and all others, or we might lump all these data into the conventional platform class. Here we report experiments with only one type of data so that some of the

$$\lambda_o = (\lambda_{\text{CONV}}, \lambda_{\text{AMB}}, \lambda_{\text{SPD}}, \lambda_{\text{NRCS}}) \tag{5}$$

are set to zero. Usually the observation function is given by the sum of squared differences between simulated (i.e., calculated from the analysis) and data values normalized by the estimated observation (and representativeness) error(s). For example, for conventional data,

$$J_{\text{CONV}} = \sum \frac{(u_a - u_o)^2}{s_u^2} + \frac{(v_a - v_o)^2}{s_u^2}. \tag{6}$$

Here (u_a, v_a) is the analyzed wind interpolated to the observation locations, (u_o, v_o) is the observed wind, and s_u is the wind component error standard deviation.

The horizontal interpolation is either bilinear or bicubic using a 12-point mask, following Ritchie et al. (1995, their Fig. 2). Since the interpolated value is a linear function of the data values at the grid points, we simplify the adjoint calculation by formulating the interpolation as a weighted sum of gridpoint values. Interpolating in one dimension and then in the other shows the weight for a grid value is the product of the weights for interpolating in each single dimension. In a single dimension, the weights are most easily determined from the Lagrangian multiplier representation of the collocating polynomial,

$$f(x) = \sum_j \left[\prod_{i \neq j} \frac{x - x_i}{x_j - x_i} \right] f_j, \tag{7}$$

where f_j are the data at locations x_j. The sum and product in (7) are from 1 to $N + 1$, where N is the order of the polynomial. [Note that when x is equal to one of the x_j, the weights in (7) reduce to one for j and zero otherwise.]

If observation errors within the data class are correlated *in a known way*, these correlations can be accounted for as described by Thépaut et al. (1993a) by setting $J_{\text{CONV}} = \mathbf{Z}^{\text{T}}\mathbf{O}^{-1}\mathbf{Z}$. Here $\mathbf{Z}$ is the vector of normalized departures, and $\mathbf{O}$ is the matrix of observation error correlations. An entry for each wind component of each observation would be contained in $\mathbf{Z}$. In the 2DVAR experiments reported here, observation error correlations are ignored since our knowledge of these statistics is limited. Currently s_u is taken to be a constant 1 m s^{-1} and knowledge of the observation error standard deviation is absorbed into λ_{CONV}.

For scatterometer data, we use either the observed backscatter values or the retrieved scatterometer wind ambiguities. The original formulation of H84 uses two observation functions—J_{AMB} and J_{SPD}—for the wind ambiguities. At each WVC,

$$J_{\mathrm{AMB}} = \sum s_{\mathrm{NSCAT}}^{-2} \prod_{k=1}^{K} d_o^2[1 - \exp(-d_k^2/d_o^2)], \quad (8)$$

where the sum is over all ambiguities, and

$$d_k^2 = (u_a - u_k)^2 + (v_a - v_k)^2. \quad (9)$$

Here K is the number of ambiguities, k is the index of the ambiguities, (u_k, v_k) is the kth wind ambiguity, d_k is the magnitude of the vector difference between analysis and ambiguity k, d_o is the wind speed scale for the observation, and s_{NSCAT} is the wind component standard deviation for the WVC. The typical value for s_{NSCAT} is 1 m s^{-1}. The wind speed scale, d_o, is defined by

$$d_o = V_o/\gamma. \quad (10)$$

Here V_o is the representative wind speed for the observation, and γ is the scaling factor for the wind speed. The typical value for γ is 2. The variability in wind speed among ambiguities for a single WVC is relatively small (H84). Therefore, the representative wind speed V_o is defined as the mean wind speed over the K ambiguities. For a single WVC, when the analysis is close to one of the ambiguities, the misfit measured by J_{AMB} approximates the squared vector differences between the ambiguity closest to the analysis and the analysis. Away from the ambiguities J_{AMB} approaches a constant.

The wind speed observation function is designed to take advantage of the relatively unambiguous wind speed information in scatterometer data. In analogy to (6) we define J_{SPD} as,

$$J_{\mathrm{SPD}} = \sum \frac{(V_a - V_o)^2}{s_V^2}. \quad (11)$$

Here V_a is the analyzed wind speed, V_o is the observed wind speed, and s_V is the wind speed error standard deviation. For NSCAT data V_o is defined above as the mean wind speed at a single WVC, but (11) might be used for any measurement of wind speed.

The second formulation for scatterometer data uses the observed backscatter values in J_{NRCS} (15). For a single location, the misfit measured by J_{NRCS} is the likelihood function used to retrieve ambiguities. For each backscatter observation, the normalized departure is

$$z_\sigma = \frac{\sigma_o^0 - \sigma_a^0}{s_\sigma}. \quad (12)$$

Here σ_o^0 is the backscatter observation, σ_a^0 is the simulated backscatter observation, and s_σ is the standard deviation of the σ^0 observation. The σ^0 values are dimensionless ratios of radar power (backscattered/emitted), and are often reported in decibels.

A model function or forward model is used to simulate σ^0. As described in section 2, the model function calculates σ^0 as a function of wind speed and direction and the geometry and polarization of the observation. The geometry is specified in terms of the pointing direction of the antenna and the incidence angle. For NSCAT the NSCAT-2 model function is preferred.

Theoretical estimates of the standard deviation of scatterometer measurements show that

$$s_\sigma = K_p \sigma^0 \quad (13)$$

(Fischer 1972). Here K_p is a dimensionless quantity with typical values between 0.05 and 0.30. The subscript p is used because K_p is originally defined in terms of the radar power. The JPL model for the standard deviation of the NSCAT σ^0 observation extends this model to

$$s_\sigma^2 = K_{pA}(\sigma^0)^2 + K_{pB}\sigma^0 + K_{pC} \quad (14)$$

(Long et al. 1988). [For *ERS-1,-2* see Stoffelen and Anderson (1997c).] When evaluating s_σ, σ^0 may be the observed value or the simulated value. If the simulated value is used, a logarithm term should be added to the loss function to be consistent with maximum likelihood estimation theory. That is,

$$J_{\mathrm{NRCS}} = \sum [z_\sigma^2 + \ln(s_\sigma)]. \quad (15)$$

The term in brackets comes about from taking the logarithm of minus the normal probability function of σ_a^0 given σ_o^0. In practice the logarithmic term is not used. In simulation it was found to introduce a bias in the retrieved wind speeds (F. Wentz 2002, personal communication).

Alternative formulations have been suggested for the loss function for scatterometer data. Thépaut et al. (1993a) used a slightly simplified form of J_{NRCS}. Stoffelen and Anderson (1997a) describes the observation function used for operational use of *ERS-1* and *ERS-2* data at ECMWF. H84 describes a wind speed functional that is equivalent to (11) if s_V is multiplied by the factor $\sqrt{1 + V_o/V_0}$, where V_0 is a constant 2 m s^{-1}, and if V_o is defined as the rms (instead of the mean) wind speed for the ambiguities at the WVC. This has the effect of giving more weight to low wind speed reports. Note that J_{SPD} may be used in combination with J_{AMB}, or alone, if there is little or no wind direction information (e.g., Atlas et al. 1991, 1996, for SSM/I observations).

Example plots of J_{NRCS}, J_{AMB} and the ECMWF formulation are given in Fig. 1 for a single WVC. If σ^0 values are used directly in 2DVAR, the loss function due to a single WVC is the MLE (Fig. 1a). This surface shows the complexity of the highly nonlinear wind retrieval problem. Note that the center of the figure is not contoured because the values there are very large, $O(10^5)$, compared to those plotted in the vicinity of the minima, $O(10^0$–$10^2)$. The MLE has multiple minima, four in this case, which correspond to the ambiguous wind solutions. The minima are distributed in an annulus of near-minimum values at roughly the same wind speed. The four minima are not equally deep, which implies that each solution has a slightly different likelihood of being the true wind.

If ambiguous winds are used in 2DVAR, then the loss function of a single WVC is J_{AMB} (Fig. 1b). This approximation of J_{NRCS} loses some of the structure seen in Fig. 1a, but still reflects the four wind solutions as

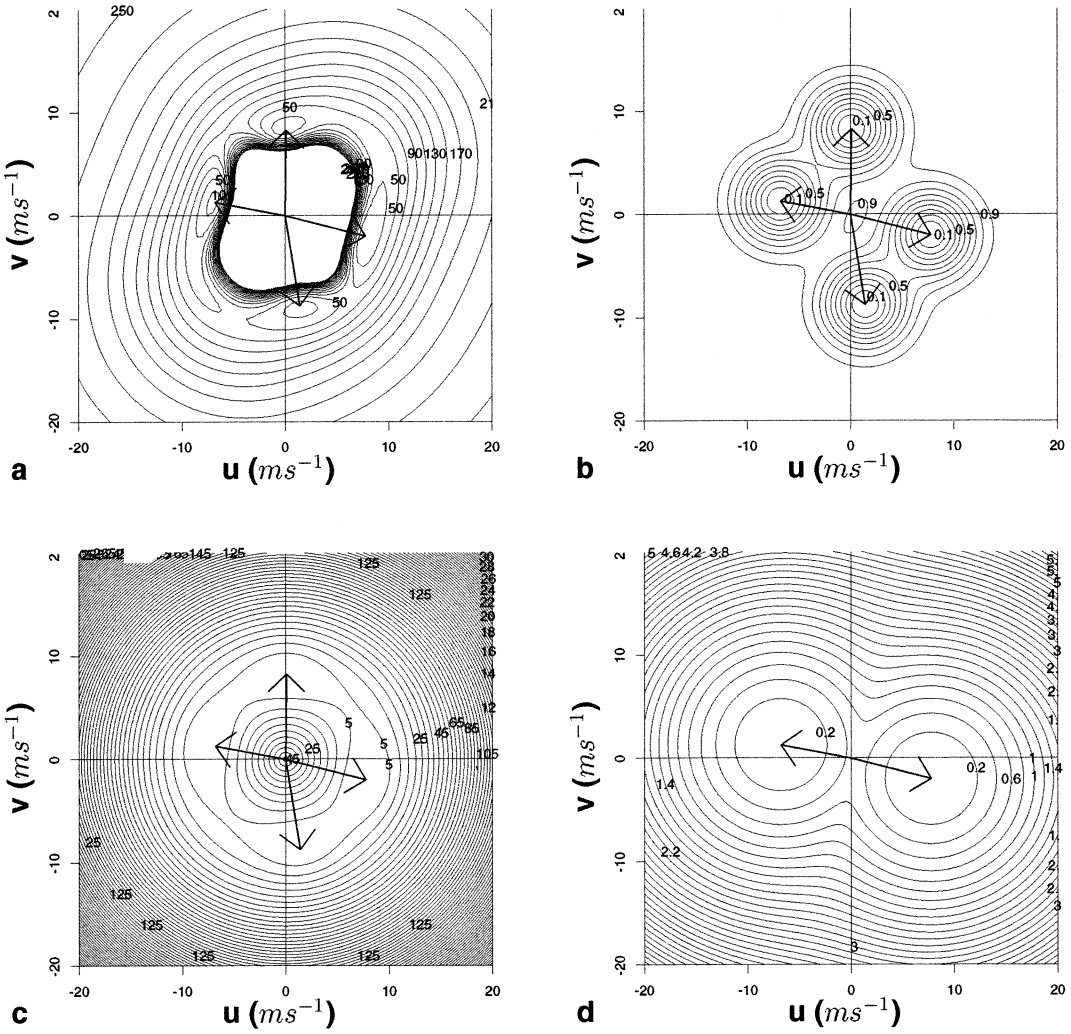

FIG. 1. 2DVAR observation operators (dimensionless) evaluated for one WVC using (a) σ^0 values directly and (b) ambiguous winds. (c) The combination of $J_{\mathrm{AMB}} + J_{\mathrm{SPD}}$. (d) For reference, the corresponding two-wind observation operator in use at ECMWF (Stoffelen and Anderson 1997a).

minima. The strong nonlinearity near the origin is removed. Note that if the background wind field is close to one of the four wind solutions, the influence of other observations or meteorological constraints will be necessary to shift the analysis from near one minimum to another during the 2DVAR minimization. Figure 1 shows that J_{AMB} is only grossly similar to J_{NRCS}, which is a precise description of the likelihood of the wind vector given the σ^0 observations. Adding J_{SPD} to J_{AMB} (Fig. 1c) improves this similarity somewhat.

The J_{AMB} formulation was originally developed for SASS for which all ambiguities were roughly equally likely. NSCAT likelihood values have significant skill for identifying the correct ambiguity. For example in Fig. 1a the eastward and westward ambiguities have deeper minima in the plot of J_{NRCS} because they are more likely. This information could be included in an ad hoc way in J_{AMB}, but our experiments show that both the J_{NRCS} and J_{AMB} formulation tend to suffer from the same deficiency, namely, that the minimizer tends to get trapped by whichever relative minimum is closest to the initial estimate. Our solution is dual ambiguity processing (section 4c).

For comparison, we also show the two-wind loss function of Stoffelen and Anderson (1997a) used at ECMWF for ERS (Fig. 1d). [A similar formulation but allowing more than two ambiguities for NSCAT is described by Figa and Stoffelen (2000).] This is the best behaved of the three functions, but it is also the crudest approximation to the MLE. Only the two most likely winds are used since one of these solutions is very close to the true wind more than 90% of the time. The smooth nature of this function allows the analysis to be moved from one minimum to another during the assimilation more easily than either the MLE or H84 formulation. However, this formulation may also permit an analysis

solution that is not very close to either minimum because of its smoothness.

b. Background constraints

As given in (2), the background function, J_b is a weighted sum of several constraints, each providing a measure of the difference between the analysis and background wind field. The simplest constraint measures the square of the vector wind magnitude:

$$J_{\mathrm{VWM}} = \frac{T^2}{L^4} \int_A (\mathbf{V}_a - \mathbf{V}_b)^2 \, dA. \tag{16}$$

The effect of J_{VWM} is to constrain the size of the analysis increments. The length and timescales, L and T, are introduced for convenience only to make the J_m nondimensional and of comparable magnitude. [If these were not concerns, these scales might be absorbed into λ_m since the adjustable parameter λ_m multiplies J_m in (2).] We use synoptic timescales and length scales, $T = 10^5$ s and $L = 10^6$ m.

The other background constraints are given by

$$J_{\mathrm{LAP}} = T^2 \int_A [\nabla^2(u_a - u_b)]^2 + [\nabla^2(v_a - v_b)]^2 \, dA, \tag{17}$$

$$J_{\mathrm{DIV}} = \frac{T^2}{L^2} \int_A [\boldsymbol{\nabla} \cdot (\mathbf{V}_a - \mathbf{V}_b)]^2 \, dA, \tag{18}$$

$$J_{\mathrm{VOR}} = \frac{T^2}{L^2} \int_A [\boldsymbol{\nabla} \cdot \mathbf{k} \times (\mathbf{V}_a - \mathbf{V}_b)]^2 \, dA, \quad \text{and} \tag{19}$$

$$J_{\mathrm{DYN}} = \frac{T^4}{L^2} \int_A \left(\left. \frac{\partial \zeta}{\partial t} \right|_a - \left. \frac{\partial \zeta}{\partial t} \right|_b \right)^2 dA. \tag{20}$$

Here (u_b, v_b) is the background wind, ζ is the relative vorticity, and $\mathbf{k}$ is the unit vertical vector. In physical terms, J_{LAP}, J_{DIV}, and J_{VOR} measure the roughness of the increments of the wind components, the irrotational wind potential function, and the nondivergent wind streamfunction, respectively. Alternatively, J_{DIV} and J_{VOR} measure the variability of the divergence and vorticity of the increments, respectively. Finally, J_{DYN} measures the variability of the analysis minus background difference of the time rate of change of the vorticity of the surface wind. Details of the calculation of J_b are given in appendix A.

c. Filtering characteristics of 2DVAR

Experiments with a single conventional wind observation show the filtering characteristics of 2DVAR. We summarize the results here, and further descriptions are given in appendix B. The nominal case is shown in Fig. 2. The reported wind is 30 m s^{-1} from 210°.

The 2DVAR solution (after sufficient iterations) is only weakly dependent on grid resolution as shown by Fig. 3. At high resolution, finite difference errors in evaluating J_b become very small and the errors due to horizontal interpolation to the observation locations in evalutaing J_o become noticeable. Bicubic interpolation should be used to avoid this. A high-resolution analysis requires greater data density and less weight given to the filtering and dynamic constraints. With this adjustment to the lambda weights, the response of 2DVAR is spatially narrower.

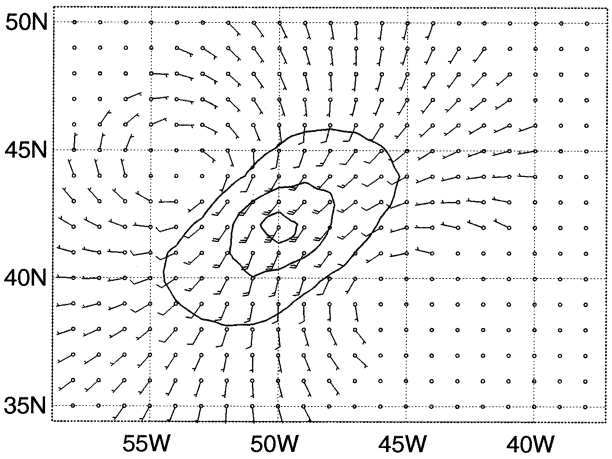

FIG. 2. Analyzed wind field for 1/2° resolution, fully converged for the nominal case described in section 3c. Here, and in the figures that follow, the wind barbs are in knots and all results are presented on a 1° grid. Wind speeds are contoured every 5 m s^{-1}.

The convergence rate of the 2DVAR minimization as presently implemented is slow, especially as resolution increases. Figure 4 shows that the number of iterations required must grow at least linearly with the number of grid intervals required to traverse the domain. Therefore the multigrid strategy of solving the same problem with increasing grid resolution initialized from the previous solution should be generally useful, and is an alternative to using a spectral representation.

4. Scatterometer quality control

a. Gross checks

Gross checking is performed when the data is read from source files and prevents nonsensical or nonphysical values from being used by 2DVAR. For example, NSCAT values of $\sigma^0 > 30$ dB are eliminated. Small negative values of σ^0 are nonphysical but are indicative of very light winds (Pierson 1989). Such values can be used in (12) with appropriately inflated K_p values, but in 2DVAR these are replaced with a small positive value equivalent to -60 dB.

b. Background and analysis checks

Background and analysis checks are done by comparing observations to simulated observations from the current analysis. At the start of the process, when the current analysis is the background, this procedure is a

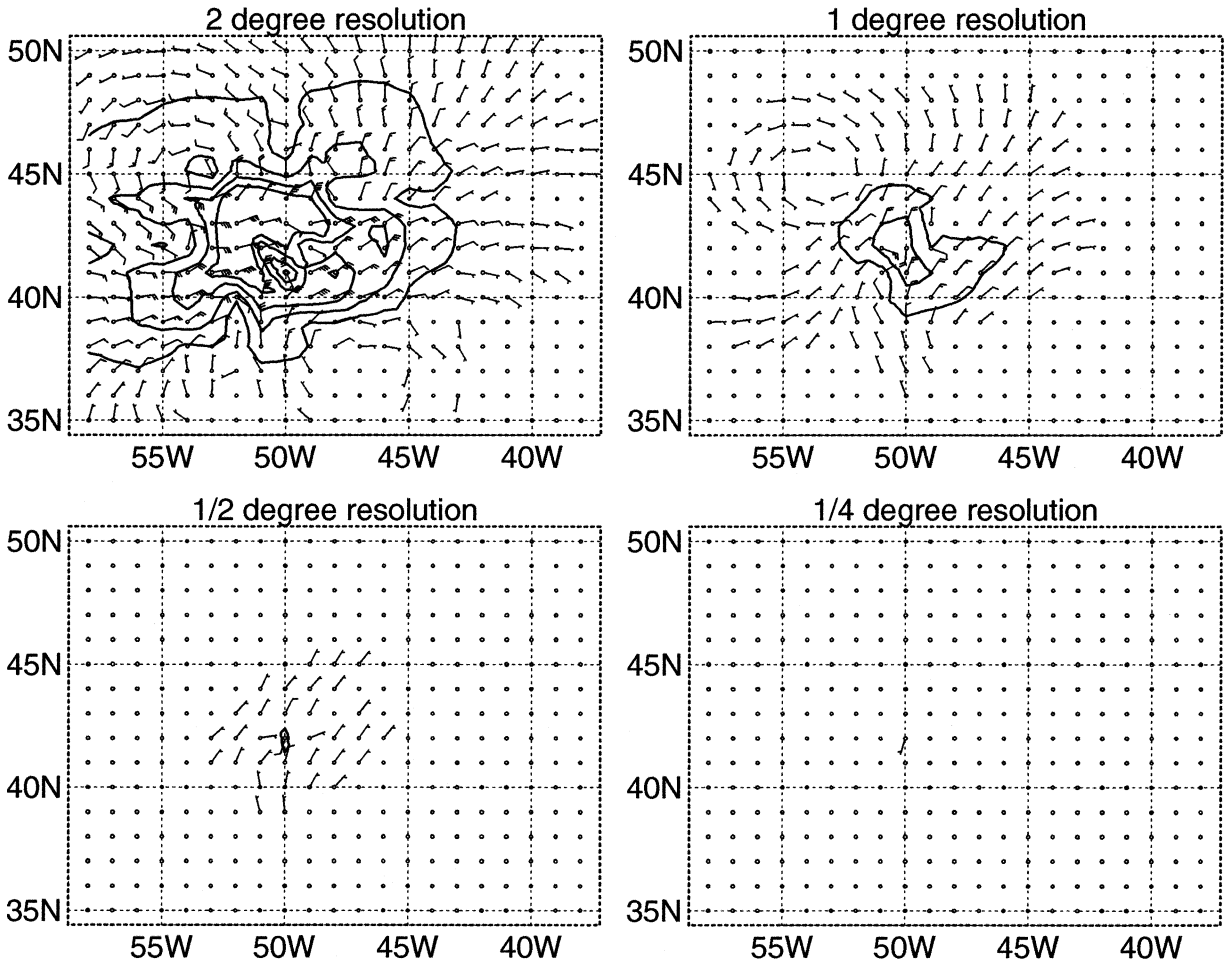

FIG. 3. Differences, scaled by 10, from the result for 1/8° resolution, for the results for 2°, 1°, 1/2°, and 1/4° resolution. The panel labeled "1/2 degree resolution" corresponds to the results shown in Fig. 2.

background check. Later it is a preliminary analysis check. Data failing the background check may be considered by a later (and more strict) analysis check. This allows some of the data eliminated by earlier QC back into the analysis.

Collocation studies show that scatterometer observation errors may be modeled in terms of wind components (Stoffelen 1998), wind vectors (Freilich and Dunbar 1999), or wind speed and direction (Atlas et al. 1999). The uncertainties exhibited in J_{NRCS} show that wind speed and direction are an appropriate context for QC. Therefore, and as in H84, if the magnitude of the difference between wind vectors (or wind speeds) is greater than the average of the observed and analyzed wind speed, the observation fails QC. If the difference between the wind directions is $>60°$, the observation fails QC. However, very small or zero winds are handled as a special case, so that when both observation and analysis indicate calm conditions, the previous checks are bypassed. The background and analysis checks apply to conventional data as well as to scatterometer winds. For ambiguities, only the ambiguity closest (i.e., with the smallest vector difference) to the current analysis is checked. For NSCAT σ^0 data, we use a simple departure test for each σ^0 measurement in decibel space,

$$\sigma_o^0 - \sigma_a^0 > \gamma_{\text{NSCAT}}. \tag{21}$$

We have used $\gamma_{\text{NSCAT}} = 9$ dB for both background and analysis checks, which typically eliminates $\sim$5% of the data.

c. Dual-ambiguity processing

Often more than two winds are retrieved for a WVC. However, one of the two ambiguities with the highest MLE values is very likely ($>$90%) to be closest to the true wind (JPL 1997). This implies that $<$10% of the third and fourth ranked ambiguities are closest to the true wind. This information can be used to QC the NSCAT data, and improve ambiguity removal.

We observed that using all available ambiguities in 2DVAR, or equivalently using the σ^0 values, leads to patches of poor ambiguity selection. This is especially true where there are four ambiguities and the direction

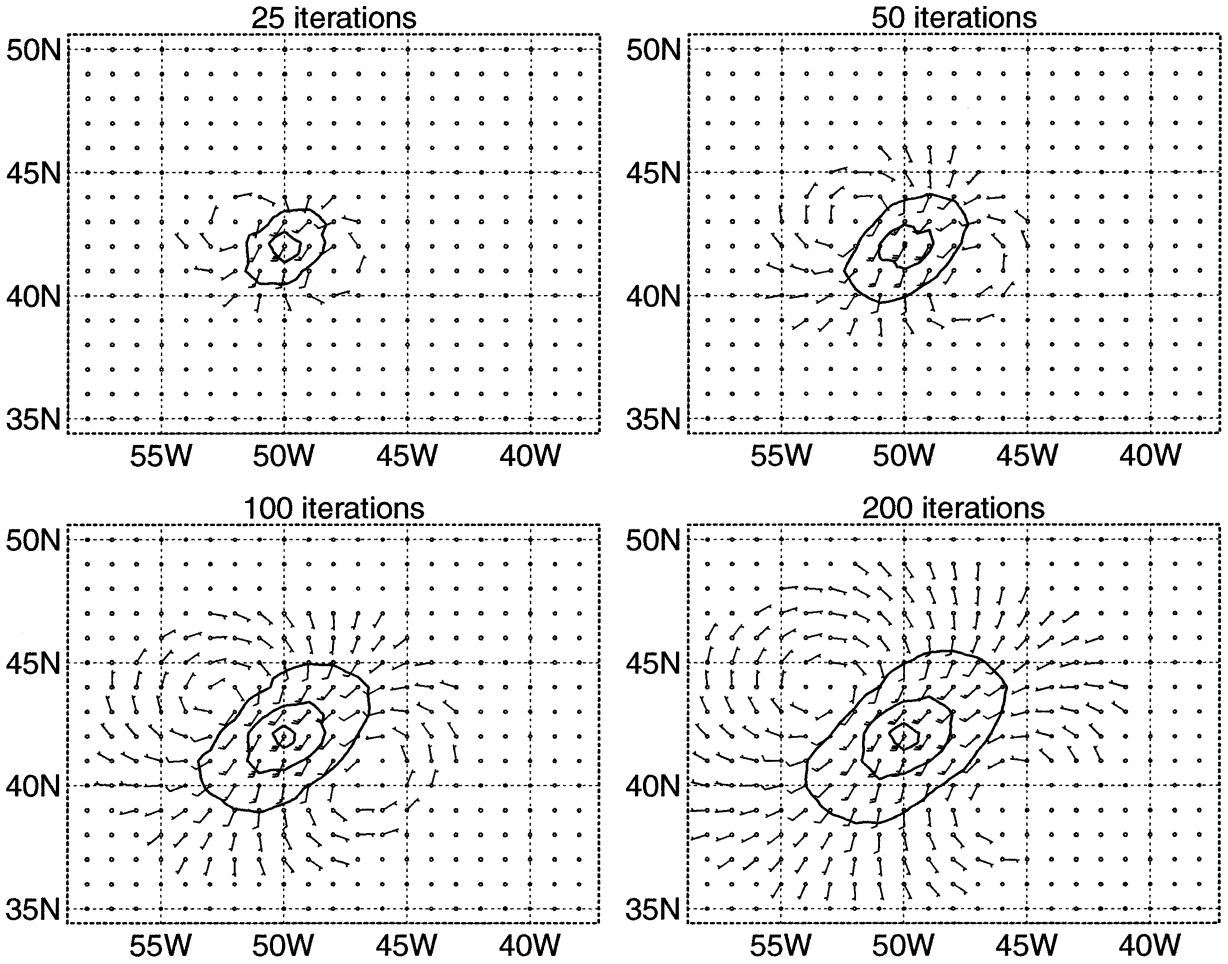

FIG. 4. The sequence of results for increasing number of iterations for 1/2° resolution, starting from a zero initial estimate.

of the third or fourth ambiguity is close to the direction of the background wind field. Using ''dual ambiguities'' (i.e., the two ambiguities with the highest MLE values) narrows the choice to one of the two most likely possibilities. This allows for larger (>45°) wind direction corrections to the background field. Using dual ambiguities only, however, naturally limits ambiguity selection to the first or second ranked ambiguity since the analysis will generally be drawn toward one or the other.

To allow for selection from all ambiguities, we have developed a two-stage analysis procedure that blends the use of dual and all ambiguities. In the first stage, we use dual ambiguities for 50 iterations of the minimizer to draw the analysis toward one of the two most likely observed winds. In the second stage, we include all ambiguities and continue to minimize until the convergence criteria are met. An alternative is to switch to σ^0 values after the first stage. The second stage allows for readjustment of the analysis in the few locations where the third or fourth ranked ambiguity is closest to the true wind.

During the first stage, we use only dual ambiguities that pass dual-ambiguity quality control or ''dual QC.'' Dual QC is based on a conceptual model of dual ambiguities. Typically, we expect the wind directions of dual ambiguities to be opposed by ~180°. If not, the retrieved winds are suspect and are not included in the first stage of dual ambiguity processing. Specifically, retrieved winds fail dual QC and are not used in the first minimization if the directions of the two most likely ambiguities are within 135° of each other. Dual QC usually eliminates ~20% of WVCs from the first minimization.

5. Use of ambiguous winds versus σ^0 observations

When using σ^0 observations, the 2DVAR method essentially carries out a simultaneous retrieval of NSCAT winds for all data presented to the analysis. While the use of J_{NRCS} is computationally more expensive that J_{AMB}, it effectively removes the WVC boundaries and links the wind retrieval problem of adjacent WVCs. (Conventional scatterometer wind retrieval solves each WVC independently.) Also, use of J_{NRCS} is a necessary

stepping stone toward simultaneous retrival of winds and ocean surface properties. (The instruments on *ADEOS-II* will take collocated active and multispectral passive microwave measurements of the sea surface. These can be used to not only improve wind retrieval, but to determine ocean surface properties as well.) If NSCAT ambiguous winds and σ^0 data represent the same geophysical information, namely, ocean surface wind stress, we expect 2DVAR to produce similar wind analyses using either data source. If this is correct, separate sets of lambda weights for ambiguous wind and σ^0 data that produce similar analyses should exist. To determine such lambda weights for ambiguous winds and σ^0 data, we vary the lambda weights, and examine the misfit of the resulting analysis to the median filter–selected ambiguity.

In these examples, we vary the lambda weights, but the comparisons cannot tell us the optimal weights. A comparison with independent data would be needed for that. Note that differences between wind-based and σ^0-based analyses will also arise for other reasons. First, quality control decisions made for σ^0 and wind data may result in different data being used. Second, WVCs with no ambiguities may contain valid σ^0 data. Third, the ambiguous wind observation loss function, J_{AMB}, is an approximation to the σ^0 data loss function (J_{NRCS}) (cf. Figs. 1a and 1b). The first two reasons will only affect a small fraction of the data presented to 2DVAR while the third reason may effect all data to a small degree. With respect to the second reason, note that a single σ^0 value is not sufficient to infer a set of ambiguities but is sufficient to refine the background wind in 2DVAR. With respect to the third reason, the σ^0 loss function (J_{NRCS}) will permit a wider variety of wind directions and a smaller range of wind speeds in the minimizing analysis compared to the ambiguous winds loss function (J_{AMB}), because of the shapes of the functions surfaces. That is, J_{NRCS} has an annulus of minimum values (all wind directions) with secondary local minima embedded while the minima in J_{AMB} are more clearly separated in direction. To maximize the similarity of J_{AMB} and J_{NRCS} we do not use dual-ambiguity processing in these experiments.

To evaluate the analysis fit to the data, we use the rms wind speed difference between the 2DVAR analysis interpolated to NSCAT WVCs and the median filter–selected ambiguity. For two North Atlantic cases, Hurricane Lili in the western Atlantic on 19 September 1996 and a cyclone west of Ireland on 27 October 1996, analyses using ambiguous winds and σ^0 data were created using a range of lambda weights. In these experiments a $1^\circ \times 1^\circ$ grid over an area 20° latitude × 20° longitude is centered over an NSCAT data swath. The background field is linearly interpolated in time to the average time of the NSCAT data from 6-hourly NCEP 1000-hPa wind analyses. The λ_m for background constraints are held fixed for all analyses at

$$(\lambda_{\mathrm{VWM}}, \lambda_{\mathrm{LAP}}, \lambda_{\mathrm{DIV}}, \lambda_{\mathrm{VOR}}, \lambda_{\mathrm{DYN}})^T = (1, 1, 4, 1, 16)^{\mathrm{T}}.$$

The minimizations were allowed to run until the gradient test was satisfied (with $\epsilon = 10^{-3}$). The lambda weights used for the winds and σ^0 analyses are

$$\lambda_{\mathrm{AMB,NRCS}} = \frac{1}{1024}, \frac{1}{256}, \frac{1}{64}, \frac{1}{16}, \frac{1}{4}, 1, 4, 16, 64, 256, 1024.$$

Smaller lambda weights for scatterometer data required fewer iterations to reach convergence (typically 10–30), and larger lambda weights required more (200–600). The stronger constraint imposed by larger lambda weights (>4) often caused the minimization to fail, since a new search direction could not be found to reduce the cost function any further. Since the minimizer is solving a problem with multiple minima, many solutions have the potential to be a local minimum. But the large decrease (>90%) and asymptotic behavior of the observation cost function values (J_{AMB} or J_{NRCS}) during the minimization suggests that dramatically lower minima probably do not exist.

Figure 5 shows the rms analysis − NSCAT observations difference as a function of lambda weight for both ambiguous wind (*w*) and σ^0 (*s*) analyses for the 27 October case. For very small lambda weights, the analyses of wind and σ^0 data are scarcely changed and fit the wind observations equally poorly (~4 m s^{-1}). For large lambda weights (>4), the analyses of wind and σ^0 data fit the wind observations much more closely, and again, equally (~1.5 m s^{-1}). The lower limit of the rms fit is governed by our choice of λ_m for the background constraints. If the background constraints were weakened (i.e., smaller λ_{VWM}, λ_{LAP}, λ_{DIV}, λ_{VOR}), the fit of the analysis to wind observations would improve. The lower limit of rms fit, in this case, is also dependent on the robustness of the minimizer. The minimizations in analyses with $\lambda_{\mathrm{NRCS}} \geq 1/4$ and $\lambda_{\mathrm{AMB}} \geq 256$ fail to converge sufficiently as mentioned earlier. This explains why the fit to σ^0 does not improve for $\lambda_{\mathrm{NRCS}} \geq 1$ in Fig. 5.

To illustrate that ambiguous winds and σ^0 data represent the same information, Fig. 6 shows analyses and increments for $\lambda_{\mathrm{AMB}} = 4$ and $\lambda_{\mathrm{NRCS}} = 1/4$ for the case of 2230 UTC 27 October 1996. The upper panels show 2DVAR analyses and the lower panels show analysis increments amplified by 10. The analyses are very similar in pattern and magnitude. While the analysis domain rms vector magnitude is 3.144 m s^{-1} for the wind-based analysis increments and 2.198 m s^{-1} for the σ^0-based analysis increments, it is 1.856 m s^{-1} for the difference of the two analyses. Differences between the analyses are subtle compared to the analysis increments. The center of the low is displaced very slightly to the east in the ambiguous winds analysis relative to the background and the σ^0 analysis. Also, in the region south of Ireland, winds from the southwest in the background are changed to more southerly winds in the ambiguous winds anal-

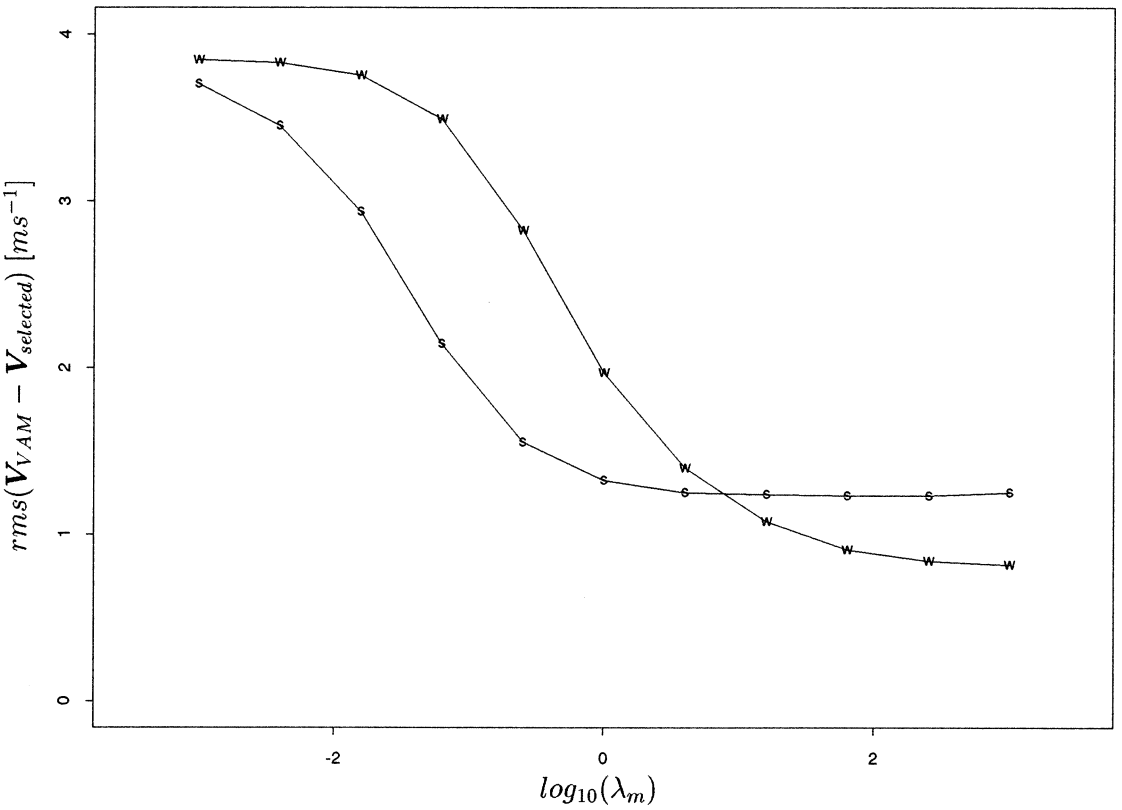

FIG. 5. The rms fit of analyses to NSCAT wind observations as a function of $\log_{10}(\lambda)$ weight for the 27 Oct 1996 case (rev 1025). Curves for analyses using ambiguous wind (*w*) and σ^0 (*s*) observations are shown.

ysis (easily seen in the increments, lower panels). This change produces a circulation pattern around the cyclone that is slightly less circular than in the σ^0 analysis. This is very likely due to the difference in the observation loss functions, that is, that J_{NRCS} tends to allow any solution within the annulus of minimum values. Apart from these minor differences, it is clear that wind and σ^0 data, while handled very differently by 2DVAR, produce nearly the same result given an appropriate choice of λ_{AMB} and λ_{NRCS}.

6. Dual-QC ambiguity removal examples

To show the usefulness of 2DVAR with dual QC for ambiguity removal, we compare our results to JPL ambiguity removal results based on the NWP-initialized or ''nudged'' median filter. 2DVAR winds and median filter winds agree in a large proportion of the WVCs, usually 95% or more. Note that 2DVAR uses ECMWF analyses as backgrounds while the JPL median filter is nudged with NCEP analyses. For a 51-day period, Henderson et al. (2003) present detailed statistical comparisons of the 2DVAR versus JPL-selected ambiguities obtained by using the same NCEP analyses in 2DVAR as the JPL product. They also present comparisons for the whole NSCAT mission for the 2DVAR ambiguity selections based on the ECMWF backgrounds.

In cases of disagreement both sets of winds are still horizontally coherent. In our synoptic evaluation, we find 2DVAR winds tend to be more meteorologically reasonable. Recall that both methods are nonlinear and have multiple solutions. Because 2DVAR requires dynamic consistency and the median filter does not, solutions of the median filter are not necessarily solutions of 2DVAR. For example, two blocks of winds with opposite directions can satisfy the median filter, but not 2DVAR.

As a test of our dual-QC procedure we initially processed 234 orbits of NSCAT data based on the NSCAT-1 model function during the period 15 October–5 November 1996. JPL and 2DVAR ambiguity selection differences are predominately at lower wind speeds (Table 1). To further assess the performance of 2DVAR, we use *GOES-8* imagery to locate mesoscale meteorological features in the North Atlantic, for the subset of 29 orbits passing over the North Atlantic when the sun elevation angle was sufficient to make use of the GOES visible channel (Grassotti et al. 1999). We examined 11 North Atlantic scenes where JPL and 2DVAR ambiguity selection differed. From the 11 scenes, 29 subregions were examined in detail. For brevity, we present one of the subregions below and then summarize the results of all 29.

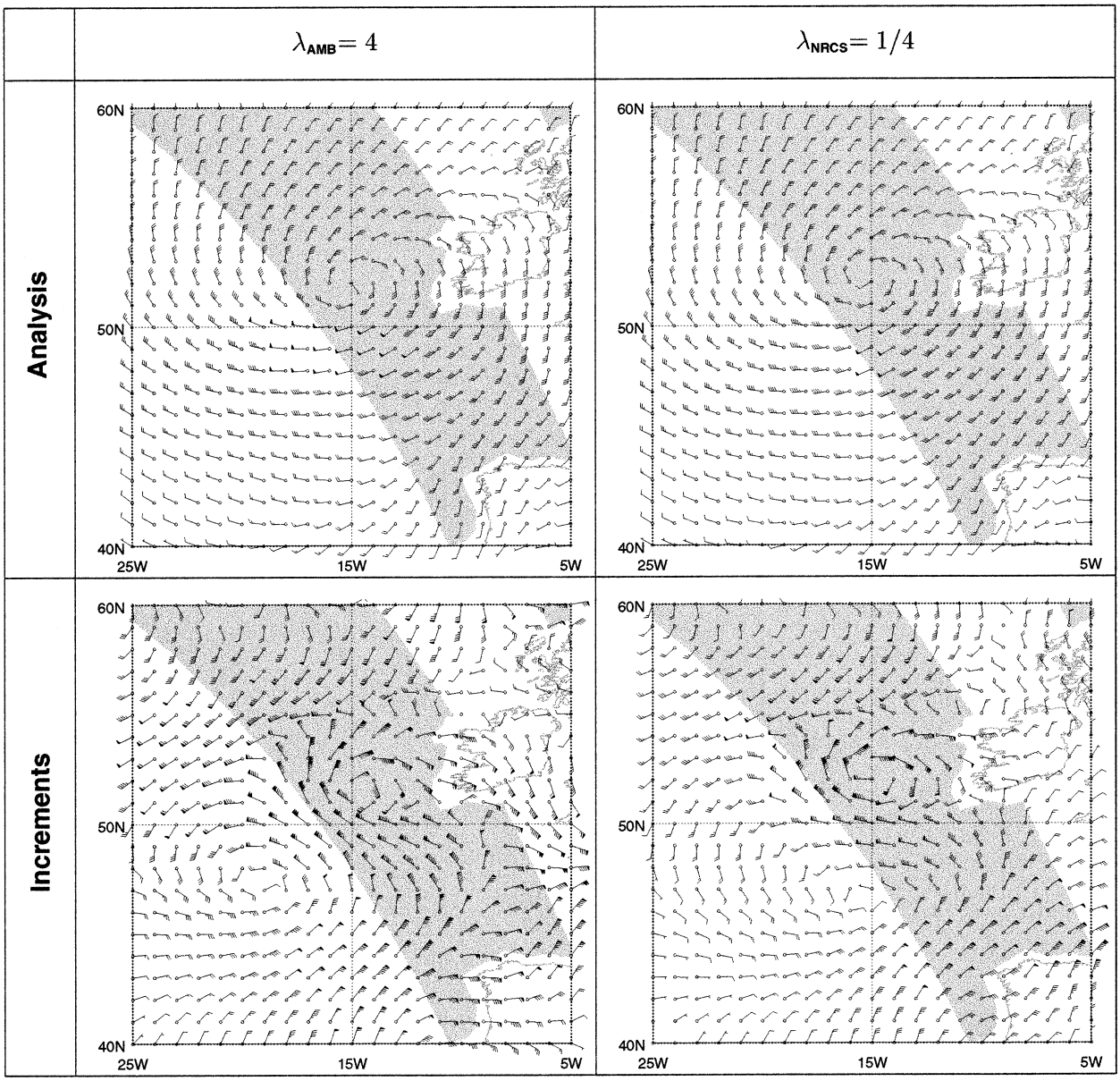

FIG. 6. Comparison of VAM analyses using (left) ambiguous winds ($\lambda_{AMB} = 4$) and (right) σ^0 observations ($\lambda_{NRCS} = 1/4$), valid at 2230 UTC 27 Oct 1996. (top) Analyses and (bottom) analysis increments (analysis minus background times 10). NSCAT swaths are shaded.

TABLE 1. Differences between JPL and 2DVAR ambiguity selection as a function of wind speed for 15 Oct–5 Nov 1996. The column labeled *N* gives the number of comparisons in each wind speed bin.

Wind speed (m s^{-1})	*N*	Percent difference
0–2	260 521	18.379
2–4	836 017	11.169
4–16	5 867 770	3.807
>16	142 815	1.438
All	7 107 123	5.141

a. Case of 26 October 1996

At 1314 UTC 26 October 1996 NSCAT passed 30°N traveling toward the equator in the North Atlantic. Differences between JPL and 2DVAR-selected ambiguities occur in small patches near (29°N, 35°W), (41°N, 37°W), (45°N, 30°W), and (57°N, 32°W). Although most of the ambiguities agree we focus on one of these patches of disagreement near a mature cyclone at 41°N, 36°W. Figure 7 shows ECMWF (magenta barbs) and 2DVAR (black barbs) wind analyses in this area over an image of *GOES-8* IR brightness temperature valid at 1315 UTC 26 October 1996. NSCAT WVC locations

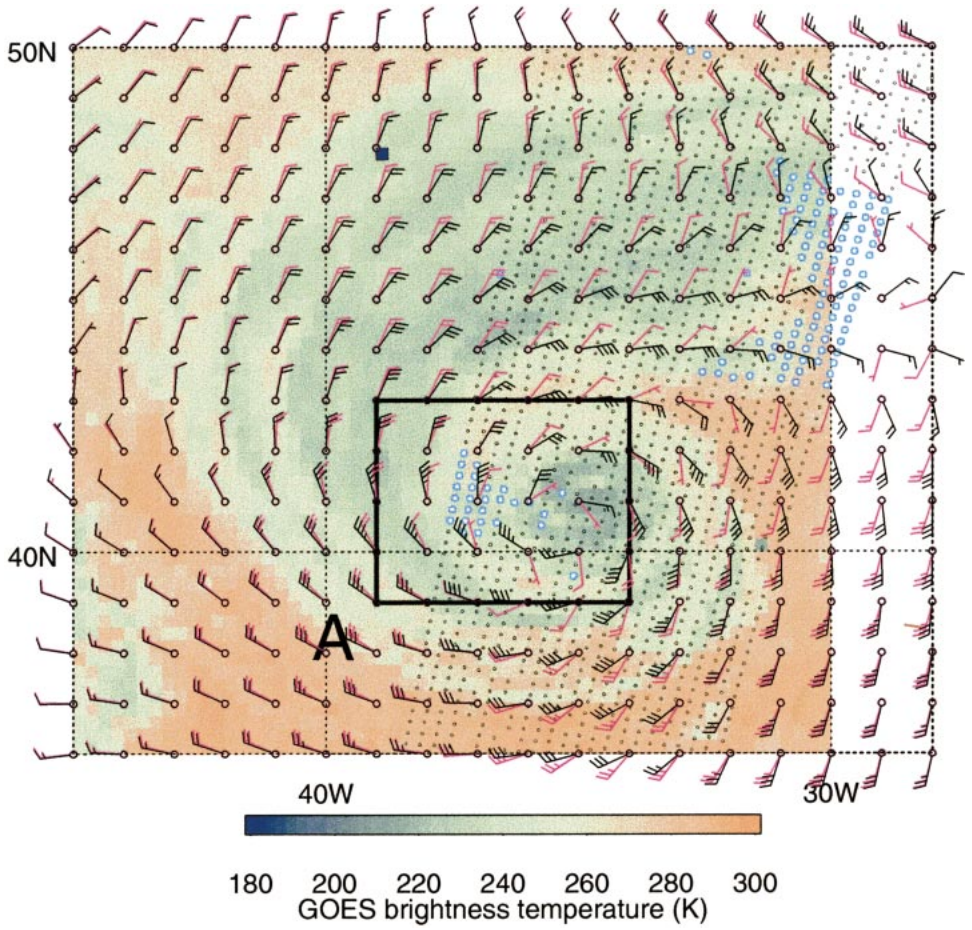

FIG. 7. ECMWF (magenta barbs) and 2DVAR (black barbs) wind analyses overlaid on *GOES-8* IR brightness temperature. NSCAT WVC locations are marked by fine black dots. Blue circles with white centers mark WVCs where JPL and 2DVAR ambiguity selection differ.

are marked by small black circles, and points where JPL and 2DVAR ambiguity selection differ are marked by larger blue circles with white centers. It is interesting to note several effects of the NSCAT data on 2DVAR surface wind analysis. The circulation center in the 2DVAR analysis is moved north and east of the center in the ECMWF analysis. The placement in the 2DVAR analysis is in better agreement with the satellite image. Also, the wind speeds around the cyclone are higher (roughly doubled) in the 2DVAR analysis than in the ECMWF analysis.

All JPL ambiguities in subregion A of Fig. 7 are plotted in Fig. 8. The ambiguous winds are consistent with a cyclone centered at 41°N, 36°W. Figure 9 shows JPL and 2DVAR-selected ambiguities for subregion A. A physically unlikely east–west wind shift exists in the JPL ambiguities in the northwest quadrant of the storm (41.5°N, 37°W) (Fig. 9a). The satellite imagery is more consistent with the circular wind flow around the cyclone center evident in the 2DVAR selected ambiguities (Fig. 9b). Note that 2DVAR positions the center of circulation ≥50 km south of the wind shift in the JPL-selected ambiguities.

b. *Summary of all cases with collocated GOES imagery*

The 29 cases where 2DVAR and JPL ambiguity selection differ that were examined include cloudy and clear scenes, Tropics and midlatitudes, and coastal and open water regions. The results from each subregion are categorized by the differences between the JPL and 2DVAR selected ambiguities. Using *GOES-8* imagery and general knowledge of the local wind field from ECMWF analyses, 2DVAR selected ambiguities are determined to be either 1) clearly improved over JPL selected ambiguities, 2) different from JPL but equally plausible, or 3) clearly worse than JPL selected ambiguities. For reference, 2DVAR-selected ambiguities were determined to be a clear improvement over JPL-selected ambiguities for the subregion presented in section 6a. For the 29 subregions we examined, 10 sub-

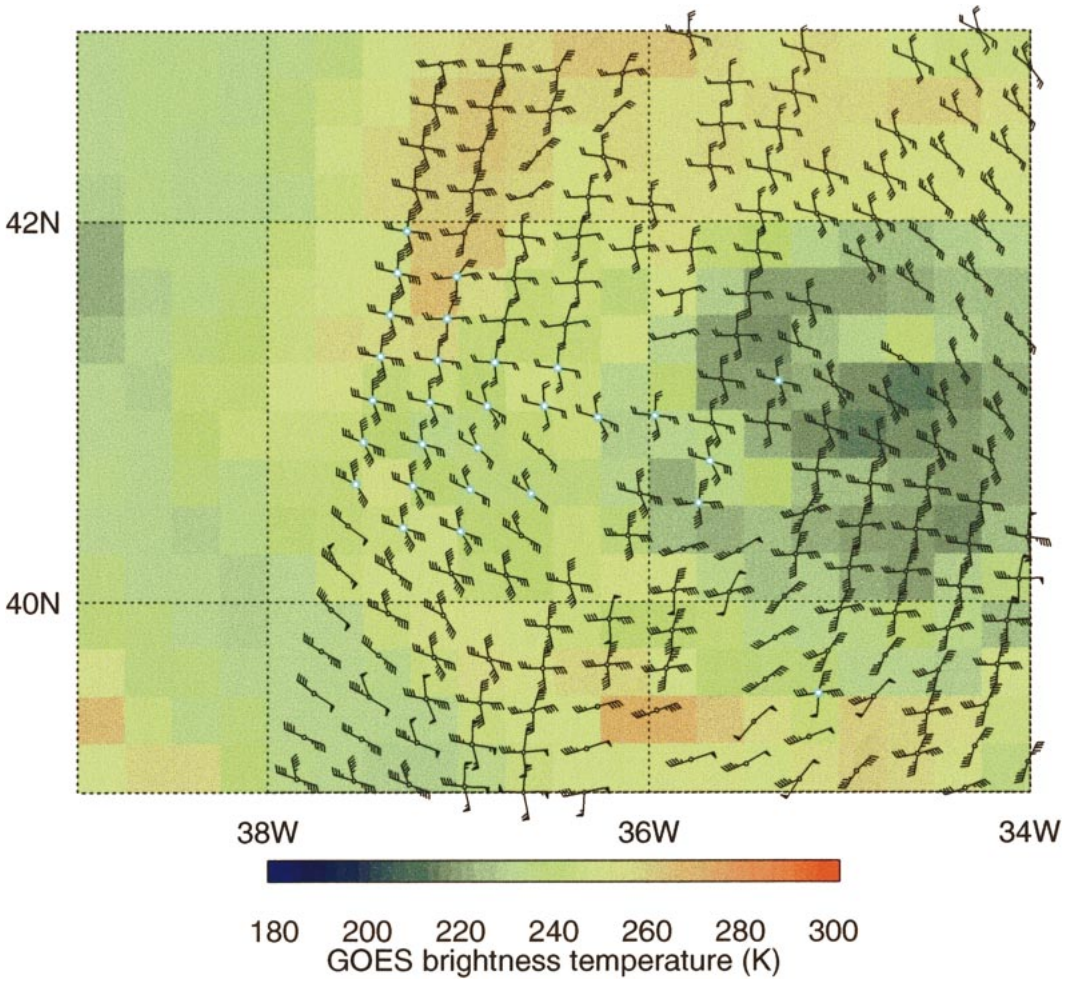

FIG. 8. All JPL ambiguities and *GOES-8* IR brightness temperature in subregion A indicated in Fig. 7. Otherwise as in Fig. 7.

regions are clearly improved over JPL-selected ambiguities; 16 subregions are different from JPL but equally plausible; and three subregions are clearly worse than JPL-selected ambiguities. Cases classified as ''equally plausible'' often occur when the evidence from the imagery is not decisive. For example, sometimes a front is aligned with a cloud feature in both 2DVAR and JPL selections but displaced one or two WVCs in the perpendicular direction. In other ''equally plausible'' cases all ambiguities are inconsistent with the imagery.

7. Concluding remarks

2DVAR provides an alternative method of ambiguity removal for NSCAT data. In this paper we describe both 2DVAR and its application to NSCAT data. 2DVAR analyses are used to select ambiguities by choosing the ambiguous wind closest to the analyzed wind field at each WVC location. Comparisons between the use of ambiguities and backscatter in 2DVAR show the near equivalence of these two data for this purpose and also demonstrate tuning the lambda weights. Whether using ambiguities or backscatter, the objective function is highly nonlinear—multiple solutions are possible. The analysis tends to settle on the ambiguity closest to the background field. When the background quality is not sufficient, the fraction of third and fourth ambiguities chosen is larger than expected: NSCAT and buoy collocations show that more than 90% of selected ambiguities should be the first or second ambiguity. This leads to the concept of ''dual-ambiguities'' processing that uses a preliminary analysis based on the two most likely ambiguities as the initial estimate for a final refined analysis based on all ambiguities.

Ambiguity removal using 2DVAR shows promise and may have advantages over median filter techniques. While JPL and 2DVAR ambiguity selection differ for only ~5% of WVCs, the differences tend to occur in patches. Patches of poorly selected winds can be more harmful to analysis and forecasting systems than scattered errors if not properly quality controlled. In ~30% of the cases examined, 2DVAR selected ambiguities are

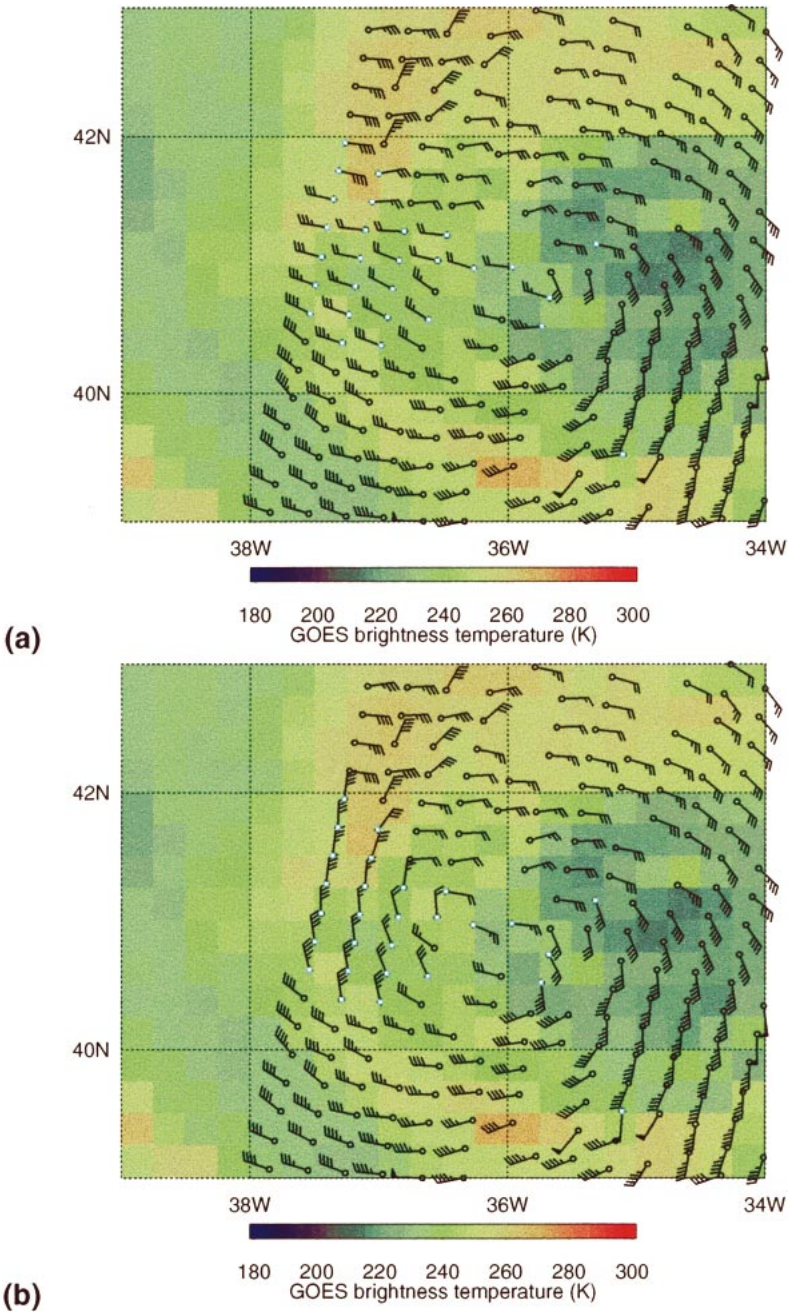

FIG. 9. (a) JPL and (b) 2DVAR selected ambiguities. Otherwise as in Fig. 8.

a clear improvement over JPL selected ambiguities. In ~60% of these cases, there was either insufficient information to determine which choice was more likely or a reasonable solution was not present in the ambiguities. In the remaining ~10% of these cases, the JPL-selected ambiguities are preferred. Note that 2DVAR used ECMWF backgrounds and JPL used NCEP backgrounds. In a companion article, Henderson et al. (2003) investigate the effect of the choice of background, and process the entire 9-month mission.

Ambiguity removal remains a difficult problem in a small but important percentage of cases involving fronts or small mobile storms associated with positional errors in the background field and/or rain contamination. Since a background field is required for effective ambiguity removal, positional errors in the background field can have a substantial effect on ambiguity selection. Scatterometer data might be used to correct such errors using the ''feature calibration and alignment'' technique (Hoffman and Grassotti 1996; Nehrkorn et al. 2003).

TABLE A1. Scales and operators for the background constraints.

m	S_m	$\mathcal{R}_m$	Q_m
VWM	$T^{-2}L^4$	$\mathbf{V}$	—
LAP	T^{-2}	$(\nabla^2 u, \nabla^2 v)$	—
DIV	$T^{-2}L^2$	$\nabla \cdot \mathbf{V}$	$\mathbf{V}$
VOR	$T^{-2}L^2$	$-\nabla \cdot \mathbf{k} \times \mathbf{V}$	$\mathbf{k} \times \mathbf{V}$
DYN	$T^{-4}L^2$	$\partial\zeta/\partial t$	$-(\zeta + f)\,\mathbf{V} - \mathbf{k} \times \mathbf{F}$

Rain contamination should be identified and removed before ambiguity removal. For NSCAT, the effect of removing flagged WVCs on ambiguity removal using 2DVAR was generally found to be small by Grassotti et al. (1999), but occasionally large differences result from eliminating just one WVC. For SeaWinds, rain effects seem to be more important. The first SeaWinds on QuikSCAT flies alone but several innovative rain flags have been developed (Jones et al. 2000; Mears et al. 2000; Boukabara et al. 2002). The advanced scanning microwave radiometer aboard *ADEOS-2* should provide an accurate rain estimate for the second SeaWinds, being readied for launch at the time of this writing.

Acknowledgments. Data used in the research reported here were provided by the Jet Propulsion Laboratory Physical Oceanography Distributed Active Archive Center, the National Center for Environmental Prediction, and the European Centre for Medium-Range Weather Forecasts. We thank the editor and the three anonymous reviewers for their considerable time and effort—the manuscript was much improved during the review process. This research was supported by the NSCAT and SeaWinds NASA scatterometer projects.

APPENDIX A

Calculation of the Background Constraints

The background constraints of section 3b are all formulated as

$$J_m = \frac{1}{S_m} \int_A [\mathcal{R}_m(\mathbf{V}_a) - \mathcal{R}_m(\mathbf{V}_b)]^2 \, dA. \qquad \text{(A1)}$$

Several of the operators $\mathcal{R}_m$ are put in the form,

$$\mathcal{R} = \nabla \cdot \mathbf{Q}. \qquad \text{(A2)}$$

In numerical experiments, we found that this version of the Laplacian leads to an instability in the minimization. Instead the Laplacian is calculated at each grid point and then J_{VWM} and J_{LAP} are calculated in the same way, by averaging four adjacent gridpoint values to estimate the value at the center of the grid box (section c, appendix A). The background constraints and scales are specified in terms of S_m, $\mathcal{R}_m$, and Q_m in Table A1. Here f is the Coriolis parameter, and $\mathbf{F}$ is the surface friction term in the momentum equation. Other terms in Table A1 are defined in section 3b.

The definitions of the Q_m for J_{DIV} and J_{VOR} follow immediately from the definitions of the $\mathcal{R}_m$ and the vector identities. To compute the dynamic constraint and to determine the Q_{DYN}, we start with the equations from Bourke et al. (1977) for the time rate of change of vorticity. We then eliminate horizontal (but not surface) friction and vertical advection terms. Horizontal friction is negligible at synoptic scales. Formally the vertical velocity in sigma coordinates is zero at the surface. The friction term $\mathbf{F}$ is calculated as in H84. An improvement would be to use the Louis (1979) boundary layer model based on Monin–Obukhov similarity theory (Monin and Obukhov 1954), and the Charnock (1955) surface roughness relationship. One would have to assume neutral stability, but the effects on ambiguity removal of this assumption would be small (Hoffman and Louis 1990).

a. Grid organization

In our implementation the grid is specified in terms of longitude and latitude denoted for convenience by the variables x and y, respectively. We evaluate all the functionals over a rectangular region in x and y. However, the data acceptance window for evaluating the J_o terms and the integration domain for evaluating the J_b terms might be specified separately. For both x and y there is a starting location, an increment δ, and a number of grid boxes n. These grid boxes are numbered from 1 to n and the corresponding grid points are numbered from 0 to n. To evaluate some of the finite difference operators and to allow higher-order horizontal interpolation, a boundary zone one grid box wide is added to the grid. The gridpoint indices therefore run from -1 to $n + 1$, and the boundary grid boxes are numbered 0 and $n + 1$. Schematically,

Grid box		0	1	2	$\cdots$	n	$n+1$	
Grid point	-1	0	1	2	$\cdots$	$n-1$	n	$n+1$

Grid points 0 and n at the integration boundary may be either active or passive, that is, allowed to vary during the minimization or held fixed. If they are held fixed, they are part of the boundary. In the experiments reported here they are active and part of the control vector. The domain may be periodic in the x direction. In this case grid points i and $i + 2\pi/\delta$ are the same. Our implementation does not allow pole points.

b. Finite differencing

Simple finite difference forms are used. If the components of $\mathbf{Q}$ are (p, q), then in spherical geometry,

$$\nabla \cdot \mathbf{Q} \approx p_x + q_y - \frac{\tan\phi}{a} q, \quad \text{and} \qquad \text{(A3)}$$

$$\nabla q = (q_x, q_y), \qquad \text{(A4)}$$

where for any p and q,

$$p_{x,ij} = \frac{p_{i+1,j} - p_{i-1,j}}{2a\ \cos(y_j)\,\delta x}, \qquad q_{y,ij} = \frac{q_{i,j+1} - q_{i,j-1}}{2a\delta y}. \quad \text{(A5)}$$

These finite difference forms are applied directly at a grid point to evaluate ζ. However, the $\mathcal{R}$ are evaluated at the center of the grid box. Instead of applying (A5) directly in (A3) at the grid points and then averaging, we apply (A3) at the center of the grid box. We evaluate $\overline{p_x}$ by first averaging in y and then differencing in x. The overbar indicates a value at the center of the gridbox. Similarly, we evaluate $\overline{q_y}$ by first averaging in x and then differencing in y. For q, we again take the average of the corner gridpoint values.

c. Evaluation of integrals

All integrals are put in the form of (A1). For J_{VWM} and J_{LAP} there are two integrals of this form—one for each wind component. We discretize each integral as

$$J_m = \sum_{i,j} (\Delta\tilde{R}_{ij})^2 A_{ij}, \quad \text{(A6)}$$

where $\Delta\tilde{R}_{ij}$ is the estimate of $\mathcal{R}_m(\mathbf{V}_a) - \mathcal{R}_m(\mathbf{V}_b)$ at the middle of grid box ij, and A_{ij} is the area of grid box ij. As mentioned for J_{VWM} and J_{LAP}, the $\tilde{R}_m$ are estimated as the average of the four corner gridpoint values. For the other constraints, the $\tilde{R}_m$ are estimated as described in appendix A, section b.

d. The gradient calculation

We identify the best analysis as the minimizer of the discrete formulation of J. Thus we may easily subsume the approximation errors introduced by the finite difference and integration formula into the assumption that minimizing J provides the optimal analysis. These considerations suggest choosing simple averaging and difference forms. However, it is vital that once the finite-difference version of J is chosen, the gradient of J be calculated as exactly and precisely as possible. In coding the adjoint it is important to note that some points in the gridded wind field are not independent. In a global field points at longitudes 0° and 360° are the same. Only one copy would be present in the control vector $\mathbf{X}$.

The calculation of J_b and its gradient is made efficient, both in terms of calculations and memory, as follows. Since both the analysis and background fields are gridded, it is possible to evaluate all of the constraints by sweeping from south to north in latitude. In addition the total background function may be considered to be the weighted sum of many partial cost functions, one for each constraint and each grid box. Since the weights are fixed and known a priori, it is possible to accumulate the contributions of these partial cost functions to the sensitivities of the total background function in the same sweep over latitude.

APPENDIX B

Response to a Single Ship Observation

Most of the results presented in this appendix are based on 2DVAR analyses for a single ship at 42°N, 50°W, observing 30 m s^{-1}, from 210°. For these experiments the background field is taken to be totally calm. The resulting analyses are essentially Green's functions, that is, the response of the analysis to a single impulse. All analyses are done on a grid large enough that boundary effects should be small. The grid runs from 290° to 330°E, and from 24° to 60°N. For graphical output we thinned (or interpolated) the analysis grid to 1° resolution in the window 302°–322°E and 35°–50°N. Most results are for

$$\lambda = (\lambda_{\text{CONV}}, \lambda_{\text{VWM}}, \lambda_{\text{LAP}}, \lambda_{\text{DIV}}, \lambda_{\text{VOR}}, \lambda_{\text{DYN}})^{\text{T}}$$
$$= (20, 1/4, 1, 4, 1, 16)^{\text{T}},$$

and the single ship observation. These λ values are identical to those used elsewhere except that J_{VWM} is given a weight of 1/4 instead of a weight of 1. Therefore, these experiments are similar to those in H84 except that less weight is given to the background, resulting in somewhat larger analysis increments. However, results of the current experiments are somewhat at odds with the earlier conclusions because H84 was overly optimistic about the convergence of the 2DVAR minimization and did not always use sufficient iterations in high-resolution experiments.

Results for the current nominal case are given in Fig. 2. The 2DVAR response is elongated in the direction of the wind observation, and at sufficient distance in the perpendicular direction, there is a return flow, most significantly to the northwest. The response is nearly 20 m s^{-1} at the observation location.

a. Effect of grid resolution

Runs were made with grid increments of 2°, 1°, 1/2°, 1/4°, and 1/8° using various methods of initialization and stopping criteria. For resolutions from 1° to 1/8° the solutions are nearly the same. That is, if everything else is fixed (weights, data, domain, . . .), 2DVAR produces the same answer independent of resolution, *if* it is allowed to iterate sufficiently. The 2° solution has somewhat jagged contours and exhibits less return flow, but is similar to the higher-resolution solutions. In Fig. 3 differences with respect to the 1/8° solution are displayed. Clearly, the solutions obtained are approaching a limit as the resolution is increased. Differences are concentrated at the observation location. These differences are small and in obtaining these results it is critical that the 2DVAR minimization has converged.

b. Convergence of the minimization

The reason for the slow convergence of the 2DVAR minimization at high resolution is illustrated by Fig. 4.

This shows the results at 1/2° resolution, beginning with a zero initial estimate, after 25, 50, 100, and 200 iterations. 2DVAR initially attempts to fit the ship observation locally. At any iteration, if a grid point currently has a zero analysis wind increment (relative to the background) and if all its neighbors do also, then all the constraints are perfectly satisfied and there will be no change during the next iteration. As a result the pattern of the solution slowly expands and grows during the iteration.

Many iterations were needed to show that the numerical solution is approaching a limiting (presumably true) solution. However for practical purposes it is sufficient to iterate 25 times at 2°, interpolate to 1°, iterate 25 more times, and continue this process to the desired resolution. We call this process regridding. Regridding with only 25 iterates per resolution step provides agreement to the most accurate solution to within 1 m s^{-1} at resolutions of 1/2° and better, and agreement to the converged solution for the same grid increment to 1 m s^{-1} or better at all resolutions.

c. Sensitivity to the lambda weights

Analyses varying the lambda weights by a factor of 4 were made using 1/2° resolution. Changing the observation weight changes the amplitude of the response, but does not change the shape or scale of the response. Increasing the filtering and dynamic constraints gives a solution of larger spatial scale, with smaller amplitude and less return flow to the right and left of the wind observation. Decreasing the weight given the fit to the background provides a generally bigger response of the same shape, but larger spatial scale, relative to the nominal case.

The half-width at half-height of the 2DVAR response to a single observation might be used to define the effective resolution of the analysis. This resolution is controlled by the weight given the filtering and dynamic constraints relative to the background constraint. On the other hand, the amplitude of the 2DVAR response can be controlled by varying λ_{CONV}. For the nominal case changing some of the λ_m by a factor of 4 results in a 25%–30% change in amplitude or scale of the response.

In general, eliminating a constraint increases the relative observation weight and hence the amplitude of the analysis. Eliminating the divergence and vorticity penalty functions gives a solution of similar spatial scale, with larger amplitude and greater return flow to the right and left of the wind observation. Eliminating the dynamic constraint results in a less elongated solution, less return flow, and larger amplitude at the observation location. Eliminating both the divergence and vorticity penalty functions and the dynamic constraint gives a very symmetric pattern with no variation in wind direction. In this case the problem for each velocity component is effectively decoupled. In the cases without the dynamic constraint, there is no dependence on the Coriolis parameter or indeed on location, and the solutions are symmetric about the line defined by the observed wind vector.

d. Effect of interpolation

We found that bilinear interpolation is adequate for most purposes. Comparing experiments in which the observation location is a grid location to experiments in which the observation is in the interior of a grid cell allows us to differentiate the effects of errors of interpolation to the observation location in evaluating J_o from the effects of finite-difference errors in evaluating J_b. Bilinear interpolation errors are the same size or smaller than finite-difference resolution errors for grid sizes larger than 1/2°. Cubic interpolation errors are small compared to the effects of finite difference errors for all grid sizes examined.

e. Solutions with two observations

A second observation at 45°N, 50°W, of 27 m s^{-1} from 350° is added to our nominal experiment. The two observations are similar to the two critical observations close to the center of the *QEII* storm studied by Hoffman (1982). The response of 2DVAR to each observation by itself is analogous to the results of the nominal case. That is, the response is aligned with the observed wind direction, and is proportional to the observed wind speed. The solution due to two observations is qualitatively in agreement with, but stronger than, the sum of the two solutions found for each observation separately.

REFERENCES

Atlas, R., S. C. Bloom, R. N. Hoffman, J. V. Ardizzone, and G. Brin, 1991: Space-based surface wind vectors to aid understanding of air–sea interactions. *EOS, Trans. Amer. Geophys. Union,* **72,** 201–208.

——, R. N. Hoffman, S. C. Bloom, J. C. Jusem, and J. Ardizzone, 1996: A multiyear global surface wind velocity data set using SSM/I wind observations. *Bull. Amer. Meteor. Soc.,* **77,** 869–882.

——, S. C. Bloom, R. N. Hoffman, E. Brin, J. Ardizzone, J. Terry, D. Bungato, and J. C. Jusem, 1999: Geophysical validation of NSCAT winds using atmospheric data and analyses. *J. Geophys. Res.,* **104,** 11 405–11 424.

Badran, F., S. Thiria, and M. Crepon, 1991: Wind ambiguity removal by the use of neural network techniques. *J. Geophys. Res.,* **96,** 20 521–20 530.

Boggs, D., 1981: The *Seasat* scatterometer model function: The genesis of SASS I. Internal Doc. 622-230, Jet Propulsion Laboratory, Pasadena, CA, 44 pp. [NTIS PD 622-230.]

Boukabara, S.-A., R. N. Hoffman, C. Grassotti, and S. M. Leidner, 2002: Physically-based modeling of QSCAT SeaWinds passive microwave measurements for rain detection. *J. Geophys. Res.,* **107,** 4786, doi:10.1029/2001JD001243.

Bourke, W., B. McAvaney, K. Puri, and R. Thurling, 1977: Global modeling of atmospheric flow by spectral methods. *General Circulation Models of the Atmosphere,* J. Chang, Ed., Methods in Computational Physics, Vol. 17. Academic Press, 267–324.

Brown, R. A., 1986: On satellite scatterometer capabilities in air–sea interaction. *J. Geophys. Res.*, **91,** 2221–2232.

Charnock, H., 1955: Wind stress on a water surface. *Quart. J. Roy. Meteor. Soc.*, **81,** 639–640.

Conradsen, K., L. B. Nielsen, and L. P. Prahm, 1984: Review of Weibull statistics for estimation of wind speed distributions. *J. Climate Appl. Meteor.*, **23,** 1173–1183.

Dee, D. P., and A. M. da Silva, 1998: Data assimilation in the presence of forecast bias. *Quart. J. Roy. Meteor. Soc.*, **124,** 269–295.

——, G. Gaspari, C. Redder, and L. Rukhovets, 1999: Maximum-likelihood estimation of forecast and observation error covariance parameters. Part II: Applications. *Mon. Wea. Rev.*, **127,** 1835–1849.

Desroziers, G., and S. Ivanov, 2001: Diagnosis and adaptive tuning of observation-error parameters in a variational assimilation. *Quart. J. Roy. Meteor. Soc.*, **127,** 1433–1452.

de Vries, J. C. W., and A. C. M. Stoffelen, 2000: 2D variational ambiguity removal. Tech. Rep. 226, Royal Netherlands Meteorological Institute (KNMI), De Bilt, Netherlands, 66 pp.

Figa, J., and A. Stoffelen, 2000: On the assimilation of Ku-band scatterometer winds for weather analysis and forecasting. *IEEE Trans. Geosci. Remote Sens.*, **38,** 1893–1902.

Fischer, R. E., 1972: Standard deviation of scatterometer measurements from space. *IEEE Trans. Geosci. Electron.*, **GE-10,** 106–113.

Freilich, M. H., and R. S. Dunbar, 1999: The accuracy of the NSCAT 1 vector winds: Comparisons with National Data Buoy Center buoys. *J. Geophys. Res.*, **104,** 11 231–11 246.

Gonzales, A. E., and D. G. Long, 1999: An assessment of NSCAT ambiguity removal. *J. Geophys. Res.*, **104,** 11 449–11 457.

Grassotti, C., S. M. Leidner, J.-F. Louis, and R. N. Hoffman, 1999: Development and application of visible-infrared rain flag for scatterometer data. *J. Appl. Meteor.*, **38,** 665–676.

Gu, C., and G. Wahba, 1991: Minimizing GCV/GML scores with multiple smoothing parameters via the Newton method. *SIAM J. Sci. Stat. Comput.*, **12,** 383–398.

Henderson, J. M., R. N. Hoffman, S. M. Leidner, J. V. Ardizzone, R. Atlas, and E. Brin, 2003: A comparison of a two-dimensional variational analysis method and a median filter for NSCAT ambiguity removal. *J. Geophys. Res.*, **108,** doi:10.1029/2002JC001307.

Hoffman, R. N., 1982: SASS wind ambiguity removal by direct minimization. *Mon. Wea. Rev.*, **110,** 434–445.

——, 1984: SASS wind ambiguity removal by direct minimization. Part II: Use of smoothness and dynamical constraints. *Mon. Wea. Rev.*, **112,** 1829–1852.

——, and J.-F. Louis, 1990: The influence of atmospheric stratification on scatterometer winds. *J. Geophys. Res.*, **95,** 9723–9730.

——, and C. Grassotti, 1996: A technique for assimilating SSM/I observations of marine atmospheric storms. *J. Appl. Meteor.*, **35,** 1177–1188.

——, J.-F. Louis, and T. Nehrkorn, 1992: A simplified view of adjoint calculations in the discrete case. Tech. Memo. 184, ECMWF, Reading, United Kingdom, 20 pp.

Jones, C. S., D. M. Legler, and J. J. O'Brien, 1995: Variability of surface fluxes over the Indian Ocean: 1960–1989. *Global Atmos. Ocean Syst.*, **3,** 249–272.

Jones, W. L., L. C. Schroeder, and J. L. Mitchell, 1977: Aircraft measurements of the microwave scattering signature of the ocean. *IEEE J. Oceanic Eng.*, **OE-2,** 52–61.

——, V. J. Cardone, W. J. Pierson, J. Zec, L. P. Rice, A. Cox, and W. B. Sylvester, 1999: NSCAT high-resolution surface wind measurements in Typhoon Violet. *J. Geophys. Res.*, **104,** 11 247–11 259; Corrigendum, **104,** 18 469.

——, M. Susanj, J. Zec, and J.-D. Park, 2000: Validation of QuikSCAT radiometric estimates of rain rate. *Proc. Int. Geoscience and Remote Sensing Symp. (IGARSS)*, Honolulu, HI, IEEE, 1229–1231.

JPL, 1997: NASA scatterometer science data product user's manual. Version 1.1. Jet Propulsion Laboratory, JPL D-12985, Pasadena, CA, 68 pp.

Legler, D. M., I. M. Navon, and J. J. O'Brien, 1989: Objective analysis of pseudostress over the Indian Ocean using a direct-minimization approach. *Mon. Wea. Rev.*, **117,** 709–720.

Liu, D. C., and J. Nocedal, 1989: On the limited memory method for large scale optimization. *Math. Program. B*, **45,** 503–528.

Long, D. G., 1993: Wind field model-based estimation of *Seasat* scatterometer winds. *J. Geophys. Res.*, **98,** 14 651–14 668.

——, C.-Y. Chi, and F. K. Li, 1988: The design of an onboard digital Doppler processor for a spaceborne scatterometer. *IEEE Trans. Geosci. Remote Sens.*, **26,** 869–878.

Louis, J.-F., 1979: A parametric model of vertical eddy fluxes in the atmosphere. *Bound.-Layer Meteor.*, **17,** 187–202.

Mears, C., D. Smith, and F. Wentz, 2000: Detecting rain with QuikSCAT. *Proc. Int. Geoscience and Remote Sensing Symp. (IGARSS)*, Honolulu, HI, IEEE, 1235–1237.

Meyers, S. D., C. S. Jones, D. M. Legler, K. F. Miles, and J. J. O'Brien, 1994: The sensitivity to parametric variation in direct minimization techniques. *Mon. Wea. Rev.*, **122,** 1632–1639.

Monin, A. S., and A. M. Obukhov, 1954: Basic regularity in turbulent mixing in the surface layer of the atmosphere. *Tr. Geofiz. Inst., Akad. Nauk SSSR*, **24,** 163–187.

Naderi, F. M., M. H. Freilich, and D. G. Long, 1991: Spaceborne radar measurement of wind velocity over the ocean—An overview of the NSCAT scatterometer system. *Proc. IEEE*, **79,** 850–866.

Navon, I. M., and D. M. Legler, 1987: Conjugate-gradient methods for large-scale minimization in meteorology. *Mon. Wea. Rev.*, **115,** 1479–1502.

Nehrkorn, T., R. N. Hoffman, C. Grassotti, and J.-F. Louis, 2003: Feature calibration and alignment to represent model forecast errors: Empirical regularization. *Quart. J. Roy. Meteor. Soc.*, **129,** 195–218.

Offiler, D., 1992: Wind retrieval and ambiguity removal. EPIPVS Project Note 9, Met. Office, Bracknell, United Kingdom, 14 pp.

——, 1994: The calibration of *ERS-1* satellite scatterometer winds. *J. Atmos. Oceanic Technol.*, **11,** 1002–1017.

Pegion, P. J., M. A. Bourassa, D. M. Legler, and J. J. O'Brien, 2000: Objectively derived daily ''winds'' from satellite scatterometer data. *Mon. Wea. Rev.*, **128,** 3150–3168.

Pierson, W. J., Jr., 1989: Probabilities and statistics for backscatter estimates obtained by a scatterometer. *J. Geophys. Res.*, **94,** 9743–9759.

Ritchie, H., C. Temperton, A. Simmons, M. Hortal, T. Davies, D. Dent, and M. Hamrud, 1995: Implementation of the semi-Lagrangian method in a high-resolution version of the ECMWF forecast model. *Mon. Wea. Rev.*, **123,** 489–514.

Schroeder, L. C., W. L. Grantham, E. M. Bracalente, C. L. Britt, K. S. Shanmugam, F. J. Wentz, D. P. Wylie, and B. B. Hinton, 1985: Removal of ambiguous wind directions for a Ku-band wind scatterometer using three different azimuth angles. *IEEE Trans. Geosci. Remote Sens.*, **GE-23,** 91–100.

Schultz, H., 1990: A circular median filter approach for resolving directional ambiguities in wind fields retrieved from spaceborne scatterometer data. *J. Geophys. Res.*, **95,** 5291–5304; Corrigendum, **95,** 9783.

Shaffer, S. J., R. S. Dunbar, S. V. Hsiao, and D. G. Long, 1991: A median-filter-based ambiguity removal algorithm for NSCAT. *IEEE Trans. Geosci. Remote Sens.*, **29,** 167–174.

Stoffelen, A., 1998: Toward the true near-surface wind speed: Error modeling and calibration using triple collocation. *J. Geophys. Res.*, **103,** 7755–7766.

——, and D. Anderson, 1997a: Ambiguity removal and assimilation of scatterometer data. *Quart. J. Roy. Meteor. Soc.*, **123,** 491–518.

——, and ——, 1997b: Scatterometer data interpretation: Estimation and validation of the transfer function CMOD4. *J. Geophys. Res.*, **102,** 5767–5780.

——, and ——, 1997c: Scatterometer data interpretation: Measure-

ment space and inversion. *J. Atmos. Oceanic Technol.,* **14,** 1298–1313.

Thépaut, J.-N., R. N. Hoffman, and P. Courtier, 1993a: Interactions of dynamics and observations in a four-dimensional variational assimilation. *Mon. Wea. Rev.,* **121,** 3393–3414.

——, D. Vasiljevic, P. Courtier, and J. Pailleux, 1993b: Variational assimilation of conventional meteorological observations with a multilevel primitive-equation model. *Quart. J. Roy. Meteor. Soc.,* **119,** 153–186.

Wahba, G., and J. Wendelberger, 1980: Some new mathematical methods for variational objective analysis using splines and cross validation. *Mon. Wea. Rev.,* **108,** 1122–1143.

——, D. R. Johnson, F. Gao, and J. Gong, 1995: Adaptive tuning of numerical weather prediction models: Randomized GCV in three- and four-dimensional data assimilation. *Mon. Wea. Rev.,* **123,** 3358–3369.

Wentz, F. J., 1991: A simplified wind vector algorithm for satellite scatterometers. *J. Atmos. Oceanic Technol.,* **8,** 697–704.

——, and D. K. Smith, 1999: A model function for the ocean-normalized radar cross section at 14 GHz derived from NSCAT observations. *J. Geophys. Res.,* **104,** 11 499–11 514.

——, S. Peteherych, and L. A. Thomas, 1984: A model function for ocean radar cross sections at 14.6 GHz. *J. Geophys. Res.,* **89,** 3689–3704.